[AMERICAN JOURNAL OF SCIENCE, VOL. 317, FEBRUARY, 2017, P. 177-215, DOI 10.2475/02.2017.02]

HYDROTHERMAL ALTERATION OF MAGMATIC ZIRCON RELATED TO NaCl-RICH BRINES: DIFFUSION-REACTION AND DISSOLUTION-REPRECIPITATION PROCESSES

WEI TERRY CHEN*,**,† and MEI-FU ZHOU**

ABSTRACT. **Magmatic zircon from altered gabbros adjacent to the ~1.07 Ga Lala Fe-Cu deposit, SW China was modified by NaCl-rich brines related to the Fe-Cu mineralization. The modified zircon grains are composed mostly of both inclusion-free and porous domains, and some grains also have overgrowth/rims. The inclusion-free domains, commonly overgrown by the porous domains, are roughly homogeneous under BSE imaging but display oscillatory or sector zoning under CL imaging. In contrast, the porous domains are distinctly mosaic-like under CL imaging, and contain abundant pores and mineral inclusions such as thorite, xenotime, REE-rich phases, actinolite, albite, biotite and calcite.**

The inclusion-free domains have concentrations of "non-formula" elements (for example Al, Ca, and Fe) much higher than the magmatic zircon, and are thus interpreted to be products of interaction between magmatic zircon (possibly metamictized) and the fluids via a diffusion-reaction process. However, these resultant domains have retained the Th and U contents, REE patterns, U-Pb ages and Hf isotopes of the precursor, magmatic zircon. On the other hand, the porous domains have stoichiometric end-member compositions (that is lowered Th, U, REE, Y, and P), and given that they are porous and inclusion-rich, we proposed that they have formed from the precursor, element-rich inclusion-free domains or magmatic zircon via a fluid-induced dissolution-reprecipitation process. It is notable that the porous domains retained the $^{177}Hf/^{176}Hf$ ratios of the precursors, but possess modified and meaningless U-Pb ages. Instead, a meaningful U-Pb age (1006 ± 62 Ma), similar to the timing of the Lala deposit, is well recorded by the overgrowth/rims with distinctly high LREEs (La = 50–700 ppm) and elevated Hf isotopic ratios. Our new results reveal that in the presence of the NaCl-rich brines, the nature of the precursor, magmatic zircon (that is high element budgets and/or metamictization) plays a key role on hydrothermal alteration of zircon.

Keywords: Zircon, hydrothermal alteration, diffusion-reaction, dissolution-reprecipitation, U-Pb age, Lala deposit

INTRODUCTION

Zircon is widely used for U-Pb age dating because of its high closure temperature (>900 °C) for the U-Pb system, and the very low diffusivity of U, Th, and Pb in most geological environments (Lee and others, 1997; Cherniak and Watson, 2000). However, it was demonstrated that original zircon can be modified by metamorphism and/or hydrothermal alteration, during which its U-Pb system may be partially or fully reset (for example, Cherniak and Watson, 2000; Rizvanova and others, 2000; Geisler and others, 2003; Tomaschek and others, 2003; Martin and others, 2006, 2008; Rubatto and others, 2008). Therefore, understanding the behavior of primary zircon under different conditions is important for a precise interpretation of the chemical and isotopic data of zircon (Corfu and others, 2003; Hoskin and Schaltegger, 2003; Geisler and others, 2007; Martin and others, 2008; Gerdes and Zeh, 2009; Campbell and others, 2014; Van Lankvelt and others, 2016).

* State Key Laboratory of Ore Deposit Geochemistry, Institute of Geochemistry, Chinese Academy of Sciences, Guiyang 550002, China.

** Department of Earth Sciences, University of Hong Kong, Pokfulam Road, Hong Kong, China.

† Corresponding author: chenwei@mail.gyig.ac.cn

Previous studies of element mobilization in zircon were concerned mostly with high- or low-grade metamorphic rocks (for example, Tomaschek and others, 2003; Geisler and others, 2007; Martin and others, 2008; Hay and Dempster, 2009a; Taylor and others, 2014). According to these studies, modification of zircon related to metamorphism involved either solid-state diffusion-reactions or dissolution-reprecipitation processes with the involvement of fluid phases (Putnis, 2002; Geisler and others, 2003; Tomaschek and others, 2003; Schneider and others, 2011). In recent years, alteration of zircon related to relatively low-temperature hydrothermal mineralization or sedimentary environments was also documented (for example, Geisler and others, 2007, Hay and Dempster, 2009b; Schneider and others, 2012), and it was further demonstrated that even the primary zircon was variably modified, meaningful U-Pb ages of multiple hydrothermal or metamorphic events are likely recorded in the altered zircons (for example, Kerrich and King, 1993; Campbell and others, 2014; Kempe and others, 2015; Van Lankvelt and others, 2016). However, these studies do not provide unambiguous information about compositions of the reacting fluids, and potential factors (for example, temperature, deformation, metamictization) that are important for enhancing alteration of zircon under low-temperature hydrothermal conditions (for example, Geisler and others, 2007; Martin and others, 2008). Clearly addressing these issues is important for understanding how, and to what extent, elemental and isotopic (for example, U-Pb, Hf and O) systems of primary zircon are modified during low-temperature hydrothermal alteration (for example, Gerdes and Zeh, 2009), in particular if individual zircon grains were affected by multiple growth and alteration processes.

In order to address the above issues, this study focuses on zircon from altered gabbros adjacent to the Lala Fe-Cu deposit in SW China. These altered gabbros contain zircon grains with unusual internal textures that are different from typical magmatic zircon (Chen and others, 2013). We examine the internal textures of these zircon grains in detail, and speculate that they may have formed during hydrothermal alteration related to the Lala deposit. We obtained elemental and U-Pb-Hf isotopic compositions of different types of zircon grains (or domains) in order to understand the origin and timing of these unusual zircon grains, and examine possible modification of elemental and isotopic systems of the zircon. Furthermore, potential factors that are important for enhancing alteration of zircon under low-temperature hydrothermal conditions are discussed.

GEOLOGICAL BACKGROUND

Regional Geology

South China consists of the Yangtze Block in the northwest and the Cathaysia in the southeast. The Yangtze Block is bounded by the Cathaysia Block to the southeast, the Indochina Block to the southwest, the Tibetan Plateau to the west, and the Qinling-Dabie Orogenic Belt to the north (fig. 1). In the Kangdian region, that is the southwestern part of the Yangtze Block, Precambrian rocks are dominated by Proterozoic volcanic-sedimentary sequences including the Paleoproterozoic (~1.7 Ga) Hekou, Dahongshan, and Dongchuan Groups (Chen and Chen, 1987; Hu and others, 1991; Greentree and Li, 2008; Zhao and others, 2010; Chen and others, 2013), and the late Meso- to early Neoproterozoic (~1.1 to ~0.95 Ga) Huili, Kunyang, and Julin Groups (Li and others, 1988; Greentree and others, 2006; Geng and others, 2007; Sun and others, 2009; Chen and others, 2014). The Paleoproterozoic sequences were commonly intruded by slightly younger gabbroic plutons (1.65–1.7 Ga, Zhao and others, 2010; Guan and others, 2011; Zhao and Zhou, 2011). Both the Paleoproterozoic strata and gabbroic plutons were metamorphosed to upper greenschist-lower amphibolite facies (Li and others, 1988), which was suggested to be related to the Neoproterozoic

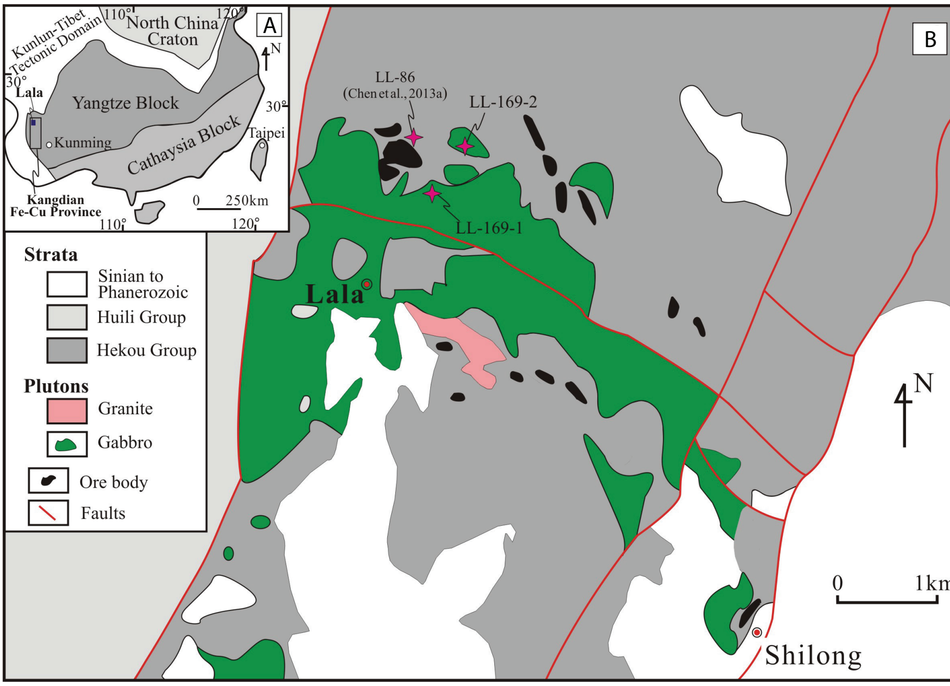

Fig. 1. (A) Tectonic framework of China showing locations of the Kangdian Fe-Cu province and the Lala Fe-Cu deposit. (B) A simplified geological map of the Lala area showing the locations of the Lala deposit and gabbroic plutons (modified after Chen and Zhou, 2012). Also shown in (B) are the sampling sites of the altered tuff and gabbros.

subduction in the region at 0.95 to 0.74 Ga (Zhou and others, 2002, 2006). On the other hand, the late Meso- to early Neoproterozoic sequences underwent only lower greenschist facies metamorphism (Chen and Chen, 1987; Li and others, 1988).

Lala Fe-Cu Deposit and Altered Gabbros

Numerous hydrothermal Fe-Cu deposits are hosted in the Paleoproterozoic Dahongshan, Dongchuan and Hekou Groups, forming the giant Kangdian metallogenic province (Sun and others, 1991; Zhao and Zhou, 2011; Zhou and others, 2014). The Lala Fe-Cu deposit, located in the northern part of the metallogenic province, is hosted in albitite, marble, and schist, and, to a lesser extent, in quartzite and meta-tuff of the Hekou Group (fig. 1B). It was well indicated that this deposit has a mineralization sequence of early Fe and late Cu-(Mo, REE) stages (Chen and Zhou, 2012). The Fe stage consists of mainly magnetite and apatite associated with pervasive alteration of albite, chlorite, and amphibole. The late, Cu-(Mo, REE) stage has a mineral assemblage of pyrite, pyrrhotite, chalcopyrite, bornite, molybdenite, carbonate, K-feldspar, and micas. The Fe-Cu mineralization has molybdenite Re-Os and allanite U-Pb ages of ~1.07 Ga (Chen and Zhou, 2012, 2014), synchronous with the 1.1 to 1.0 Ga magmatism in the Kangdian region (for example, Chen and others, 2014). Both the hosting strata and Fe-Cu ores are foliated or metamorphosed due to upper greenschist-lower amphibolite facies metamorphism possibly related to the Neoproterozoic subduction (Chen and Zhou, 2012), and locally the Fe-Cu ores are tightly deformed or mobilized, forming abundant veins composed mainly of chalcopyrite, pyrite, bonite, biotite and quartz (Chen and Zhou, 2012). These veins have biotite Ar-Ar and allanite U-Pb ages of ~0.83 Ga (Chen and Zhou, 2014; Zhou and others, 2014).

In the Lala mine, a ~1.7 Ga gabbroic pluton intrudes the meta-sedimentary-volcanic rocks of the Hekou Group, and is adjacent to the Fe-Cu ore bodies (fig. 1B). It is notable that the western section of the gabbroic pluton near the Fe-Cu ore bodies has undergone extensive alteration related to the Fe and Cu mineralization (Chen and Zhou, 2012). The gabbros of this section are crosscut by abundant calcite and chalcopyrite veins, and are associated with early pervasive Na-Fe alteration and later potassic-carbonate alteration. In contrast, the gabbros in the eastern part of this pluton are distal from the Lala mine, and thus are generally unaltered or only weakly altered (for example, Chen and others, 2013). However, both the altered and unaltered gabbros have locally suffered from deformation or foliation similar to the Hekou Group and Fe-Cu ores (Chen and others, 2013).

ANALYTICAL METHODS

Electron Probe Micro-Analysis (EPMA)

Major elemental measurement of the zircon was conducted at 25 kV and 20nA with a JEOL JXA8100 electron microprobe at the Guangzhou Institute of Geochemistry, Chinese Academy of Sciences, Guangzhou. The standards used include sanidine for Si, cubic zirconia for Zr, Hf and Y, magnetite for Fe, diopside for Ca, monazite for Th, apatite for P, and tugtupite for Cl. Counting times were 30 s for Zr-Lα (PETH), Si-Kα (TAP), Fe-Kα (LIF), Ca-Kα (PETH), P-Kα (PETH), and Y-Lα (PETH), 60 s for Hf-Mα (TAP) and Cl-Kα (PETH), 45 s for Th-Mα (TAP), and 15 s for F-Kα (LDE1). The limits of detection for these measured elements are 50 to 200 ppm. It is notable that some zircon grains contain abundant pore or minerals of micro-meters sizes, which may affect the EPMA data. However, such a potential effect can be reduced by carefully selecting target areas, based on high-resolution BSE maps. For example, the selected target areas are inclusion-free, generally >10 um in diameters.

LA-ICP-MS Trace Elemental Analyses

Trace elemental analyses of zircon were conducted in the Guangzhou Institute of Geochemistry, Chinese Academy of Sciences, Guangzhou. An Agilent 7500a ICP-MS coupled with a Resonetics RESOlution M-50 laser-ablation system was used. Detailed descriptions of the analytical procedures and instrumental operating conditions are available in Tu and others (2011). The 193 nm laser beam was operated at 10 Hz, resulting in a 33 μm diameter ablated pit. Zirconium was used as an internal standard to correct the inter-element fractionation during an individual analysis. Samples were measured in a short run bracketed by the external standard NIST SRM 612 with reference values taken from Pearce and others (1997). NIST SRM 614 was used to monitor the accuracy and precision of the analyses. Subsequent data reduction was carried out using ICPMSDataCal software (Liu and others, 2008). As some zircon grains contain mineral inclusions, particularly the porous domains, the target spots (>50 um in diameter) for laser ablation were carefully selected on the basis of BSE images to avoid inclusions. Accidental ablation of mineral inclusions during analyses was also well monitored through the time-resolved analytical signals (Appendix fig. A1).

LA-MC-ICP-MS U-Pb Dating

U-Pb isotopic analyses of zircon grains were conducted with a Nu Instrument multi-collector inductively coupled plasma-mass spectrometer (MC-ICP-MS), attached to the Resonetics RESOlution M-50-HR Excimer Laser Ablation System, at the University of Hong Kong, Hong Kong, China. Analyses were performed with a beam diameter of 30 μm and a repetition rate of 6 Hz. Data acquisition was started with a 30s measurement of a gas blank during the laser warm-up time. Typical ablation time was

40s for each measurement to produce 30 to 40 μm deep pits. ^{232}Th, ^{238}U, ^{235}U, ^{208}Pb, ^{207}Pb, ^{206}Pb, and ^{204}Pb were simultaneously measured in static-collection mode. Zircon standards, 91500 and GJ, were analyzed twice before and after every 10 analyses. 91500 was used for external corrections, whereas GJ was used as an unknown for quality control. The raw data was firstly reduced by the program ICPMSDataCal (Liu and others, 2008) and then was processed using the ISOPLOT program (Ludwig, 2003). Uncertainties are reported at the 1σ level. It is noted that accidental ablation of mineral inclusions during analyses was monitored through time-resolved analytical signals (Appendix fig. A2)

LA-MC-ICP-MS Lu-Hf Isotope Analyses

Zircon Lu-Hf isotopes were analyzed using a Geolas 193 nm excimer ArF laser-ablation system, attached to a Nu Plasma MC-ICP-MS, at the Northwest University, Xi'an City, China. The analytical protocol was similar to that outlined in Yuan and others (2008). A stationary spot was used with a beam diameter of ~40 μm, an 8 Hz repetition rate, and a laser power of 100 mJ/pulse. Zircon 91500, GJ-1, and Monastery, were used as reference zircon standards.

PETROGRAPHY OF MAGMATIC AND ALTERED ZIRCON

Zircon grains were separated from two altered gabbro samples (LL-169-1 and LL-169-2) (fig. 1). The altered gabbros are composed of secondary albite and actinolite with variable amounts of calcite, quartz, chlorite, epidote, apatite, zircon, magnetite, and chalcopyrite (fig. 2). These gabbros are different from the unaltered or slightly metamorphosed gabbros that are composed dominantly of plagioclase (partially altered to albite), clinopyroxene and secondary amphibole (Guan and others, 2011; Chen and others, 2013). Zircon grains from an altered tuff sample were also separated, in order to compare with those from the altered gabbros. The altered tuff consists mainly of albite, quartz, and K-feldspar with variable amounts of calcite, biotite, muscovite, chlorite, and magnetite (Chen and others, 2013).

Zircon grains were separated by adapting magnetic and heavy liquid techniques, followed by hand-picking under a bi-modular microscope. About 150 zircon grains from each sample were collected, mounted in epoxy, and polished to about half-thickness. Both backscatter electron (BSE) and cathodoluminescence (CL) images were obtained to investigate the morphologies and internal textures of the zircon grains in the epoxy mounts and thin sections. BSE images were determined at 20 kV and 10 nA with a Hitachi S-3400N Variable Pressure SEM at the Electron Microscope Unit, the University of Hong Kong, Hong Kong. CL images were obtained with a JEOL JSM-6510 SEM at the Beijing GeoAnalysis Co., Ltd., Beijing.

Unmodified Zircon

The altered gabbros contain only a small proportion of unmodified zircon grains that are all euhedral and do not show any signs of resorption (fig. 3). They are commonly clear and colorless under optical microscope (figs. 3A and 3B) and homogeneous under BSE imaging but exhibit oscillatory or sector growth zoning under CL imaging (fig. 3), similar to typical magmatic zircon. Indeed, as will be also demonstrated later, these zircon grains are chemically similar to magmatic zircon grains in unaltered gabbros distal from the Lala mine (Guan and others, 2011; Chen and others, 2013).

Altered Zircon

Most zircon grains from the gabbros are secondary and generally embayed or surrounded by hydrothermal minerals including albite, calcite, chlorite, biotite, and actinolite (fig. 2). Minor apatite and REE minerals are also present in the mineral

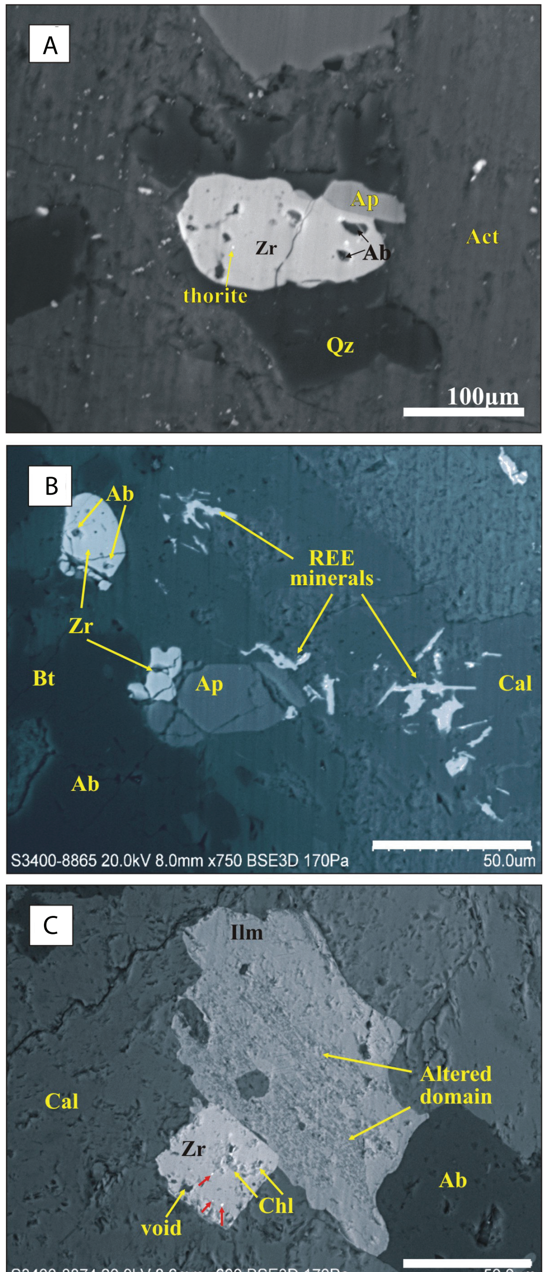

Fig. 2. BSE images of the altered gabbro showing textural relationships between zircon and other minerals. In (A) and (B), both zircon, and apatite were corroded by albite, actinolite, calcite and REE minerals. Note that the zircon grains contain various inclusions of minerals. In (C), both zircon and ilmenite grains were replaced by an matrix assemblage of calcite, albite, apatite, and chlorite. The red arrows indicate the presence of Th-HREE-Y-rich silicates in zircon. Abundant voids and chlorite is also enclosed in the zircon grain. Mineral abbreviations: Ap-apatite; Cal-carbonate; Ab-albite; Zr-zircon; Ilm-ilmenite; Mt-magnetite; Chl-chlorite; Qz-quartz; Bt-biotite; Act-actinolite.

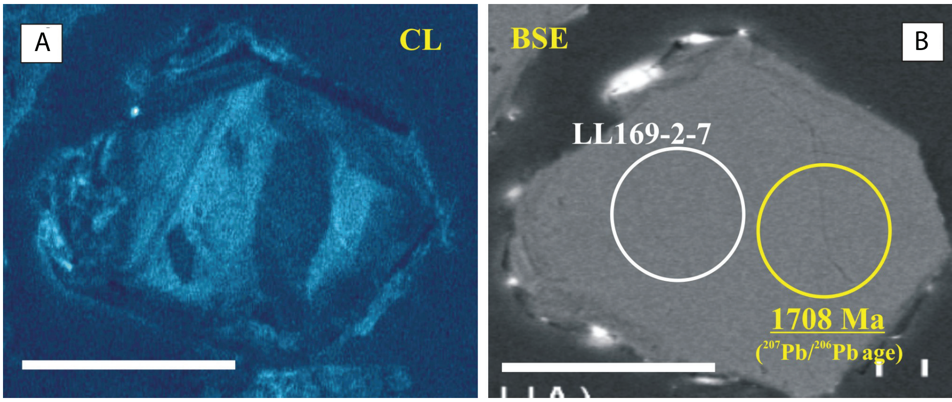

Fig. 3. Internal textures of unmodified zircon grains from altered gabbros. These zircon grains are generally euhedral, homogenous in the BSE image (B), and show oscillatory and sector growth zoning under CL image (A). Also shown are the spots for trace elemental (white circle) and U-Pb isotopic (yellow circle) analyses. The white bar refers to a length of 50 μm.

matrix surrounding the altered zircon (figs. 2A and 2B). The altered zircon grains show complex internal textures under the optical-microscopic, BSE and CL imaging (figs. 4 and 5), and generally consist of both inclusion-free and porous domains. A few altered grains also have overgrowth/rims over the porous and/or inclusion-free domains.

Inclusion-free domains.—The inclusion-free domains, mostly irregular in shape, are generally homogeneous under BSE imaging (figs. 4A, 4B, 4C, and 4D), but exhibit pronounced oscillatory or sector growth zoning under CL imaging (figs. 4B and 4D).

Porous domains.—In most cases, this kind of domain tends to occur around the inclusion-free domains with irregular and sharp contacts (figs. 4A, 4B, 4C, and 4D). They are intensively pitted and commonly were cut by angular hydrothermal minerals including albite, edenite, biotite and calcite (figs. 2B, 2C, 5C, and 5E). Under the optical microscope, the porous domains are nearly opaque due to the high density of porosity and mineral inclusions, whereas under CL imaging, they are mosaic-like with randomly distributed white and black patches (figs. 4 and 5D). The porous domains are also characterized by the presence of abundant pores or voids which are mostly irregular in shapes and generally tens of micrometers in sizes (up to 20 μm; figs. 5 and 6). It is interesting to mention that some voids contain euhedral sylvite (KCl) or halite (NaCl) as identified by using Energy Dispersive Spectrometer (EDS) (fig. 6), possibly representing relics of daughter minerals of original fluid inclusions. Such an interpretation is well supported by the local presence of crystal-bearing fluid inclusions in these domains. Other than the pores or voids, the porous domains contain abundant fine-sized, angular mineral inclusions including albite, actinolite, calcite, chlorite, HREE-Y-rich silicates, xenotime, thorite, thalenite, biotite, allanite, galena, and titanite, *et cetera* (fig. 5). These minerals are present together within a single inclusion (for example, actinolite+chlorite or calcite+biotite in a single inclusion; figs. 5E and 5G), or occur as a single-phase in relatively small inclusions (generally <5 μm), particularly for the HREE-Y-Th-rich phases such as thorite, thalenite and xenotime (figs. 5G, 5H, 5I, 6C, and 6D).

Overgrowth/rims.—Some altered grains contain overgrowth or rims over the porous domains. These rims are free of pores or mineral inclusions, and are typically homogenous and featureless under BSE images (figs. 4F, 5A, and 5B). Some rims also exhibit oscillatory zoning under CL images (fig. 4E).

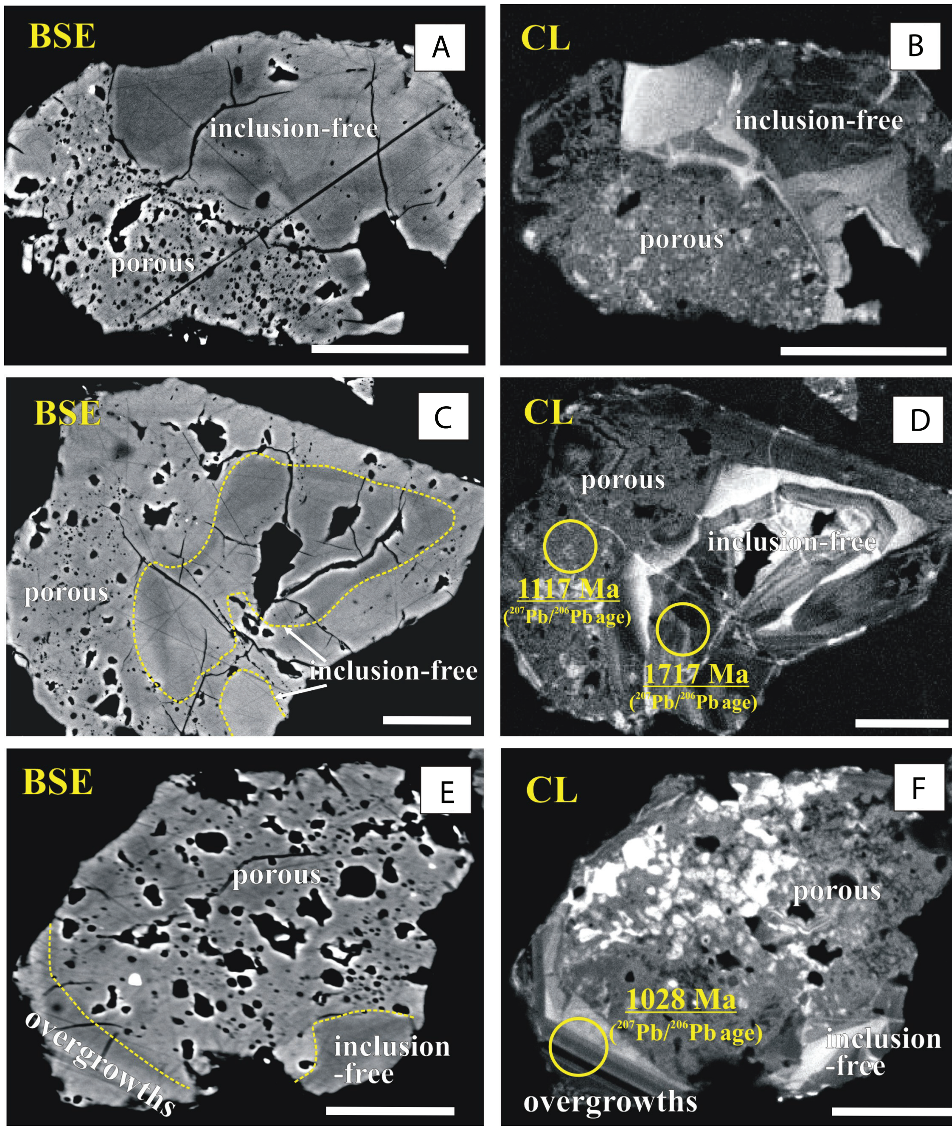

Fig. 4. BSE and CL images of several altered zircon grains from the gabbros. These zircon grains contain both the inclusion-free and porous domains, and few grains also contain overgrowth/rims over the porous domains. The inclusion-free domains are homogenous in BSE images (A, C, E) and exhibit oscillatory growth zoning in CL images (B, D), whereas the porous domains are heterogeneous and mosaic in CL images (B, D, F). The overgrowth/rims over the porous domains locally exhibit oscillatory growth zoning in CL images (F). Also shown are the sites for trace elemental (white circle) and U-Pb isotopic (yellow circle) analyses. The white bar refers to a length of 50 μm.

ELEMENTAL AND ISOTOPIC COMPOSITIONS OF ZIRCON

Representative zircon EPMA analyses are available in table 1, and the full dataset is provided in Appendix table A1. Trace elemental concentrations of the zircon are available in Appendix table A2. Moreover, their U-Th-Pb ages and Hf isotopic compositions are provided in Appendix tables A3 and A4, respectively, and illustrated in figures 7, 8, 9, 10, 11, 12, and 13 for comparison. It is notable that compared to

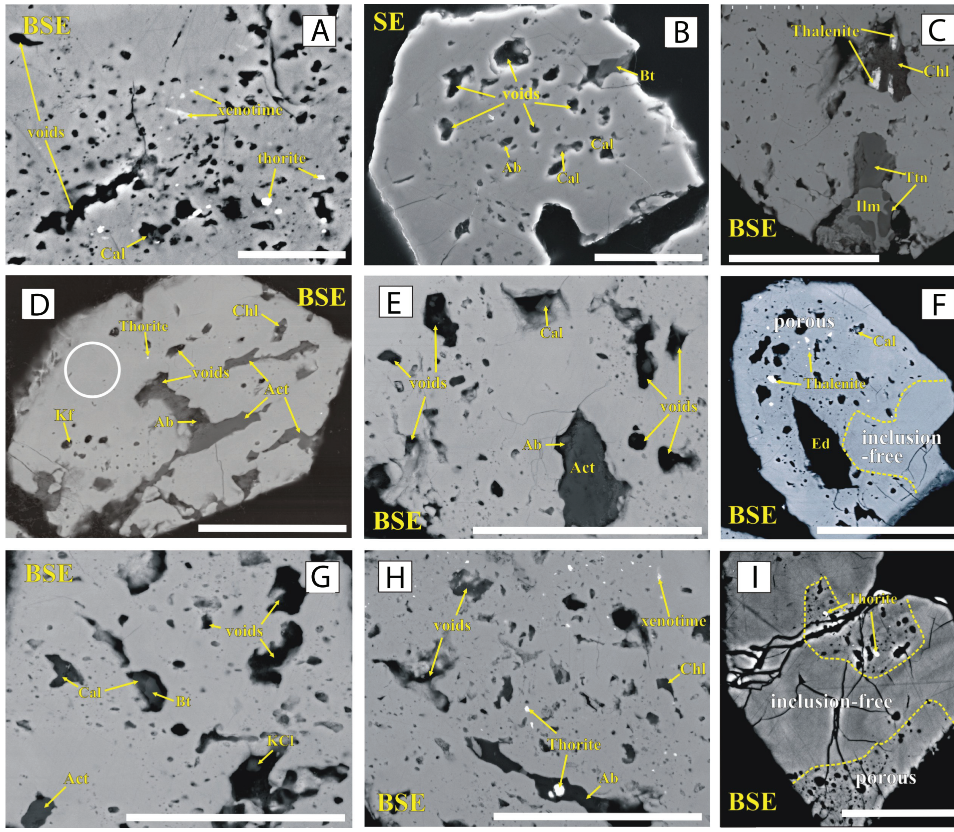

Fig. 5. Various mineral inclusions and voids in altered zircon from the gabbros. Note that these are all BSE images. The porous domain are generally embayed, and contain abundant voids and mineral inclusions including xenotime, thorite and/or other Th-HREE-rich silicates (A, C, F, H and I), albite, biotite, edenite, calcite, K-feldspar, actinolite, and chlorite (A, B, D, E, F, G, H), and ilmenite and titanite (C), Note that there is a sylvite crystal residing in one of the voids (G), possibly representing a relic daughter mineral in an original fluid inclusion. Mineral abbreviations: Cal-calcite; Chl-chlorite; Ed-edenite; Ilm-ilmenite; Ttn-titanite; Syl-sylvite; Kf-potassic feldspar; Act-actinolite. Also shown are the spots for trace elemental analyses (white circle). The white bar refers to a length of 50 μm.

EPMA analyses, trace element (also U-Th-Pb ages and Hf isotope) analyses of the porous domains are challenging, as these domains contain abundant pore or mineral inclusions. However, the possible effects of accidental ablation of inclusion were avoided by carefully selecting target spots and monitoring the time-resolved signals during analyses (Appendix figs. A1 and A2).

EPMA Compositional Data

In general, different domains of the altered zircon have more variable ZrO_2 and SiO_2 (fig. 6A) and much higher ThO_2, CaO, and FeO than the unmodified zircon (figs. 6B and 6C). Most of the inclusion-free and porous domains have total element oxide sums close to 100 weight percent, but some have totals less than 95 weight percent (Appendix table A1), possibly due to un-identified nano-sized phases or hydrous species (for example, OH) in the crystal structure. Overall, the inclusion-free domains have ThO_2 concentrations slightly higher than the porous domains but similar CaO and FeO (figs. 6B and 6C). The rims contain much lower CaO and FeO

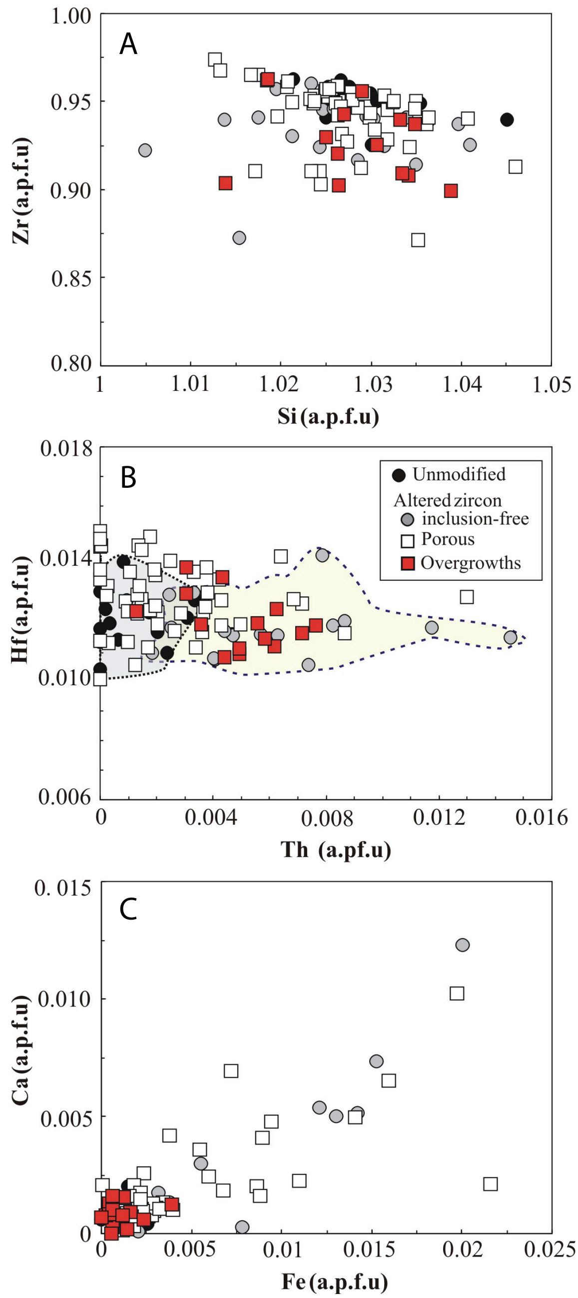

Fig. 6. Bi-modal variation diagrams showing the major elemental compositions (by EPMA) of the unmodified zircon, the inclusion-free and porous domains, and overgrowth/rims in the altered zircon grains from the altered gabbros.

contents than the porous domains (fig. 6). It is notable that both the inclusion-free and porous domains have HfO_2 contents undistinguishable from those of the unmodified zircon (fig. 6B).

Table 1

Representative electron microprobe analyses of zircons from altered gabbros

Zircon	unmodified, magmatic zircon						Inclusion-free domains					
Sample	LL169-1-21	LL169-1-26	LL169-1-27	LL169-1-35	LL169-2-22	LL169-2-26	LL169-1-11	LL169-1-15	LL169-1-16	LL169-2-6	LL169-2-21	LL169-2-29
	wt.%											
SiO_2	33.61	33.38	33.99	33.79	33.02	34.15	33.05	32.36	31.75	32.66	33.23	32.17
ZrO_2	64.60	61.48	62.64	64.50	62.17	64.17	62.66	60.45	59.73	60.43	60.18	56.67
HfO_2	1.20	1.32	1.43	1.36	1.44	1.51	1.36	1.20	1.32	1.35	1.61	1.28
ThO_2	b.d.	0.67	0.03	b.d.	0.48	b.d.	1.18	0.57	1.63	1.22	1.11	2.03
Y_2O_3	b.d.	1.61	b.d.	0.03	0.96	b.d.	0.20	0.84	1.58	0.78	1.20	2.84
P_2O_5	b.d.	b.d.	b.d.	b.d.	b.d.	b.d.	b.d.	b.d.	b.d.	b.d.	b.d.	0.23
FeO	b.d.	0.04	0.05	0.06	b.d.	0.07	0.51	0.54	0.58	0.46	0.21	0.76
CaO	b.d.	0.04	0.04	0.06	0.04	b.d.	0.15	0.15	0.22	0.16	0.09	0.36
F	b.d.	b.d.	b.d.	b.d.	b.d.	b.d.	b.d.	b.d.	b.d.	b.d.	b.d.	b.d.
Cl	b.d.	b.d.	b.d.	b.d.	b.d.	b.d.	0.12	0.14	0.14	0.03	0.04	0.12
O=F,Cl	b.d.	b.d.	b.d.	b.d.	b.d.	b.d.	b.d.	0.03	0.03	b.d.	b.d.	b.d.
total	99.43	98.54	98.18	99.82	98.14	99.92	99.19	96.22	96.91	97.08	97.67	96.43
Zircon	Porous domains						Homogeneous overgrowths					
Sample	LL169-1-8	LL169-1-19	LL169-1-22	LL169-1-34	LL169-1-40	LL169-2-1	LL169-1-3	LL169-1-42	LL169-2-2	LL169-2-8	LL169-2-30	LL169-2-37
	wt.%											
SiO_2	33.19	32.91	33.08	33.29	33.86	33.10	33.22	33.22	33.80	33.22	33.33	34.11
ZrO_2	60.81	62.55	61.34	60.67	63.60	61.60	61.77	58.93	64.37	61.16	64.58	63.32
HfO_2	1.26	1.68	1.28	1.47	1.35	1.57	1.24	1.40	1.43	1.27	1.38	1.61
ThO_2	0.24	0.25	0.14	1.86	0.52	0.53	0.70	0.88	0.18	0.88	0.80	0.44
Y_2O_3	0.94	b.d.	b.d.	0.57	0.47	0.57	1.70	2.54	b.d.	1.49	b.d.	0.65
P_2O_5	b.d.	b.d.	b.d.	b.d.	b.d.	b.d.	b.d.	b.d.	b.d.	b.d.	b.d.	b.d.
FeO	0.34	0.33	0.28	0.77	0.11	0.37	0.06	b.d.	b.d.	b.d.	b.d.	b.d.
CaO	0.12	0.06	0.21	0.31	b.d.	0.14	b.d.	b.d.	b.d.	0.04	0.03	b.d.
F	b.d.	b.d.	b.d.	b.d.	b.d.	b.d.	b.d.	b.d.	b.d.	b.d.	b.d.	b.d.
Cl	0.08	0.34	0.04	0.07	b.d.	0.09	b.d.	b.d.	b.d.	b.d.	b.d.	b.d.
O=F,Cl	b.d.	0.06	b.d.	b.d.	b.d.	b.d.	b.d.	b.d.	b.d.	b.d.	b.d.	b.d.
total	96.96	98.05	96.34	98.99	99.94	97.96	98.71	97.01	99.85	98.08	100.13	100.14

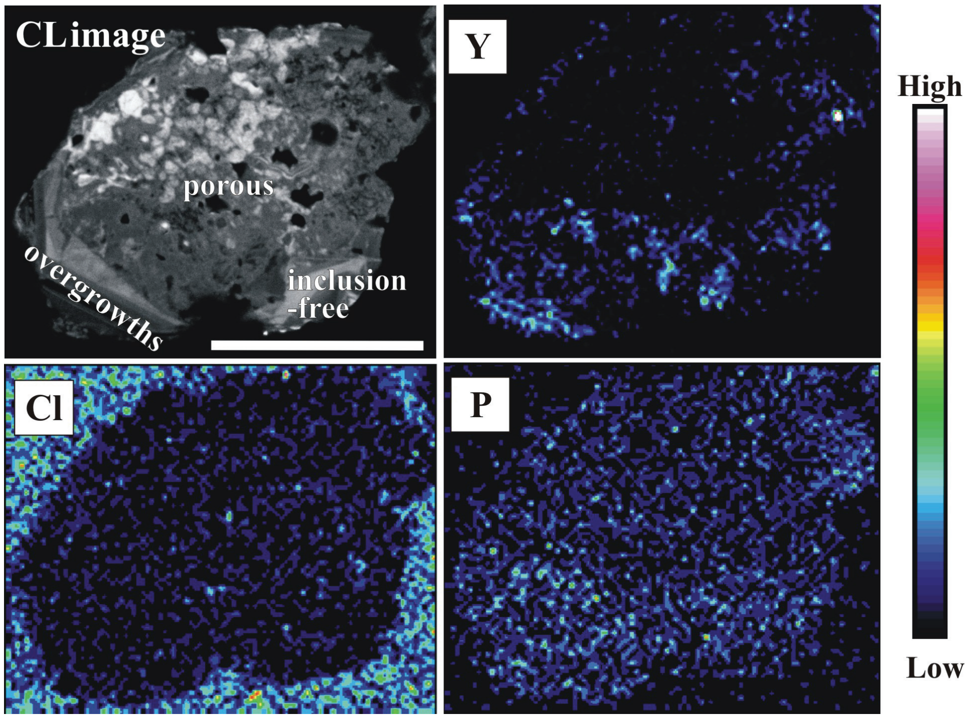

Fig. 7. Elemental distribution maps of an altered zircon from the gabbros. The inclusion-free and rims have relatively high Y and P contents.

Elemental distribution maps of selected altered zircon grains reveal that the inclusion-free domains have Y and P contents higher than the porous domains (fig. 7). The porous domains coexist with discrete Y- and Th-rich phases (for example, thorite) that are represented by bright areas in the BSE images. Note that Y and P intensities do not fully overlap, suggesting the presence of at least two different Y-rich phases, most likely thalenite and xenotime. Some relatively bright areas in the Cl-intensity map are possibly due to the presence of Cl-bearing mineral inclusions such as amphibole or biotite, as also revealed by EDS (figs. 5D, 5E, and 5G).

Trace Element Concentrations

The unmodified zircon grains have the lowest Y, P, Th, and U contents compared to different domains of the altered zircon (Appendix table A2; figs. 8A and 8B). Their chondrite-normalized REE patterns show strong enrichments in heavy REEs (HREEs) relative to light REEs (LREEs) with pronounced positive Ce and negative Eu anomalies (fig. 9A).

The inclusion-free domains have the Y, P, Th, U (>700 ppm) and total REE (mostly 5,000–12,500 ppm) contents much higher than the unmodified zircon grains (Appendix table A2; fig. 8B). However, these domains exhibit chondrite-normalized REE patterns similar to those of unmodified zircon, with similar Eu/Eu* (0.1–0.3), $(Gd/Lu)_N$ (0.1–0.5), $(Sm/La)_N$ (3–100), and Th/U ratios (1–4) (figs. 8C, 8D and 9A).

The porous domains have lower REE, Th, and U contents and $(Gd/Lu)_N$ and $(Sm/La)_N$ ratios but more LREE-depleted patterns than the inclusion-free domains

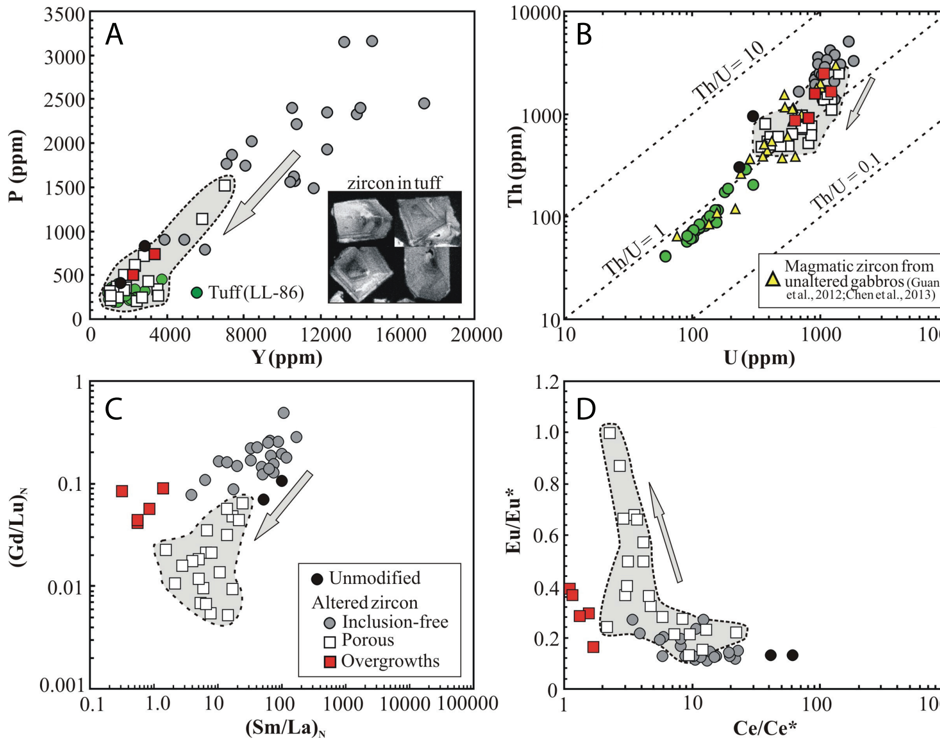

Fig. 8. Bi-modal variation diagrams showing the trace element compositions of the unmodified zircon, the inclusion-free and porous domains, and the rims of the altered zircon from the gabbros. $(Gd/Lu)_N$ and $(Sm/La)_N$ ratios are normalized to chondrite (after Sun and McDonough, 1989). The grey arrow defines the chemical changes from the inclusion-free to the porous domains. Also shown in (A) and (B) are the compositions of magmatic zircon from altered tuff in the same mine and unaltered gabbros distal to the mine (Chen and others, 2013); also shown in (A) are the CL images of the zircon from the altered tuff. Note that the zircon grains in the tuff all exhibit clear oscillatory zoning, and do not show any signs of resorption.

(figs. 8B, 8C, 8D and 9B). They have positive Ce anomalies (Ce/Ce* = 3–25) similar to the inclusion-free domains but less pronounced than those of the unmodified zircon grains (Ce/Ce* = 40–60) (figs. 8D and 9B).

The rims over the porous domains have distinctly LREE-enriched patterns with relatively high total LREE contents (530–3,300 ppm) but low $(Sm/La)_N$ ratios (0.2–2) (figs. 8C and 9C). Moreover, they have distinctly negative Eu anomalies (0.15–0.44) but slightly positive Ce anomalies (Ce/Ce*=1.1–1.7) (figs. 8D and 9C).

U-Th-Pb Ages of Zircon

U-Th-Pb isotopic data of different zircon grains or domains from the gabbros are plotted on concordia diagrams (fig. 10). The inclusion-free domains give a cluster of $^{207}Pb/^{206}Pb$ apparent ages similar to that of the unmodified zircon (Appendix table A3). All these analyses form a robust regression line with an upper intercepted age of 1723 ± 7 Ma (MSWD = 1.2) (fig. 10A).

The porous domains have a wide range of $^{207}Pb/^{206}Pb$ apparent ages from 1117 to 2103 Ma (Appendix table A3), which all plot below the concordant line for $^{206}Pb/^{238}U$ versus $^{207}Pb/^{235}U$ (fig. 10B). These plots, however, do not form a robust regression

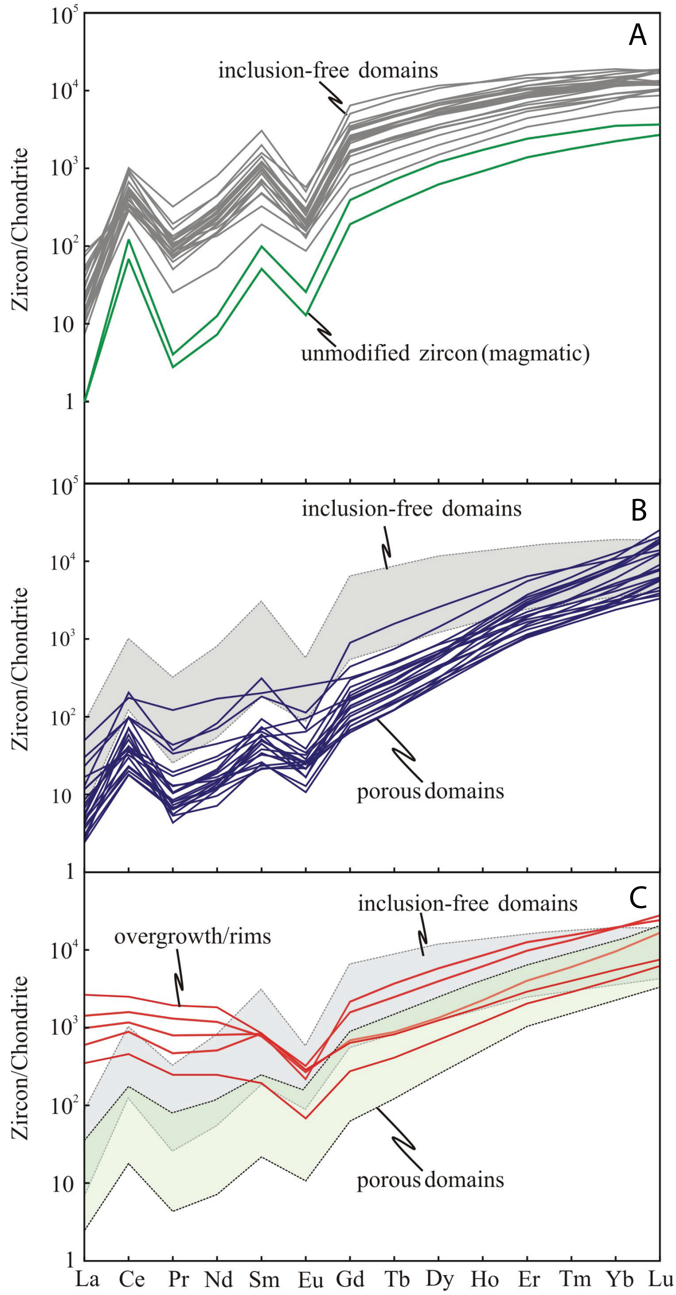

Fig. 9. Chondrite-normalized REE patterns of the unmodified zircon (A), the inclusion-free (A) and porous (B) domains, and the overgrowth/rims (C) of altered zircon from the gabbros. The chondrite values are from Sun and McDonough (1989). Note that the overgrowth/rims have distinctly high LREE contents, and exhibit relatively flat REE patterns without a pronounced Ce anomaly.

line, and some of them contain considerable amounts of common Pb (Appendix fig. A2). This is unlike the unmodified zircon, inclusion-free domains and rims, where common Pb is almost negligible (Appendix fig. A2).

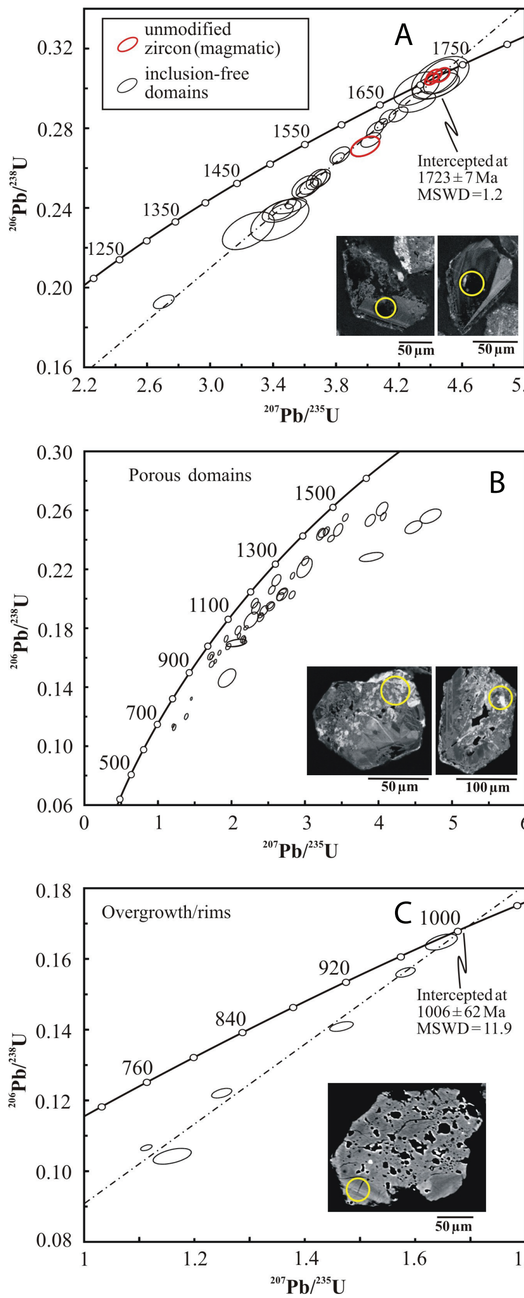

Fig. 10. U-Pb isotopic concordia plots of the unmodified (magmatic) zircon (A), the inclusion-free (A) and porous (B) domains, and overgrowth/rims (C) of altered zircon from the gabbros. Note that the inclusion-free domains have U-Pb ages similar to the unmodified (magmatic) zircon, whereas the U-Pb plots of the porous domains are all discordant but do not show a clear regression line.

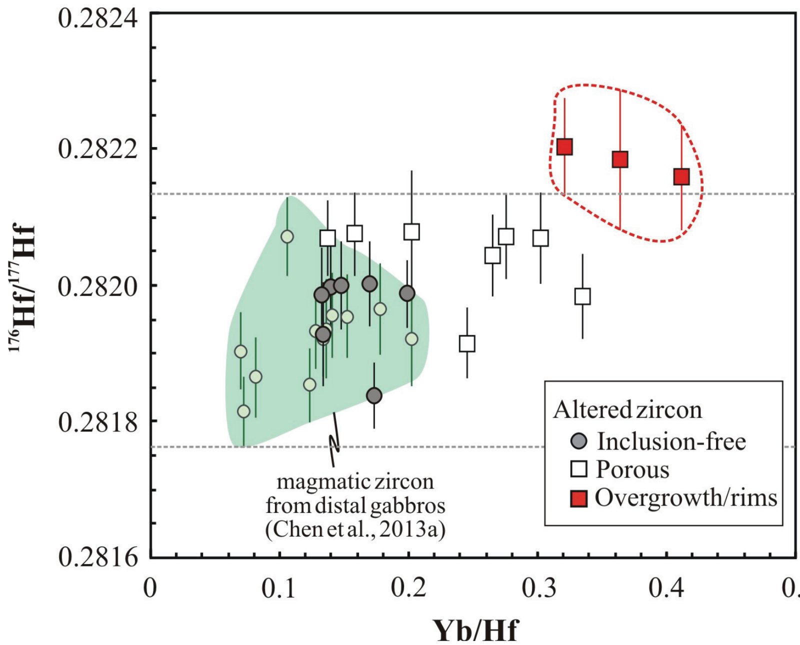

Fig. 11. Bi-modal plots of ^{176}Hf/^{177}Hf vs. Yb/Hf for the inclusion-free and porous domains, and overgrowth/rims of altered zircon grains from the gabbros. Also shown are the Hf isotopic compositions of the magmatic zircon from the unaltered gabbros distal to the Lala mine (Chen and others, 2013).

The overgrowth/rims have comparable ^{207}Pb/^{206}Pb apparent ages and form a robust regression line with an upper intercepted age of 1006 ± 62 Ma (MSWD = 11.9) (fig. 10C). This age is, within errors is similar to the molybdenite Re-Os and allanite U-Pb ages of the Lala deposit (Chen and Zhou, 2012, 2014).

Hf Isotopic Composition of Zircon

Hafnium isotopic data for different domains of the altered zircon are plotted together with previously published data for magmatic zircon from unaltered gabbros distal to the deposit (fig. 11) (Chen and others, 2013). Both the inclusion-free (0.281838-0.282002) and porous (0.281985-0.282079) domains have ^{176}Hf/^{177}Hf ratios similar to those of the magmatic zircon from the unaltered gabbros (Appendix table A4; fig. 11). Instead, the overgrowth/rims have high ^{176}Hf/^{177}Hf ratios (0.282159–0.282204) relative to both the inclusion-free and porous domains (fig. 11).

DISCUSSION

Hydrothermal Alteration of Magmatic Zircon

Formation of the inclusion-free domains via a diffusion-reaction process.—The unmodified zircon are texturally and chemically similar to typical magmatic zircon, thus representing magmatic zircon that survived from alteration of the altered gabbros. The inclusion-free domains of altered zircon also share many similarities with the unmodified or magmatic zircon in terms of internal textures, REE patterns, U-Th-Pb ages and Hf isotopic compositions (figs. 4, 8C, 9A, 10A and 11). However, their distinctly high Ca, Al and Fe concentrations (table 1 and Appendix table A2; fig. 6C and Appendix fig. A1) indicate that the inclusion-free domains are not relics of magmatic zircon. Calcium, Fe and Al are highly incompatible with the zircon structure during crystalliza-

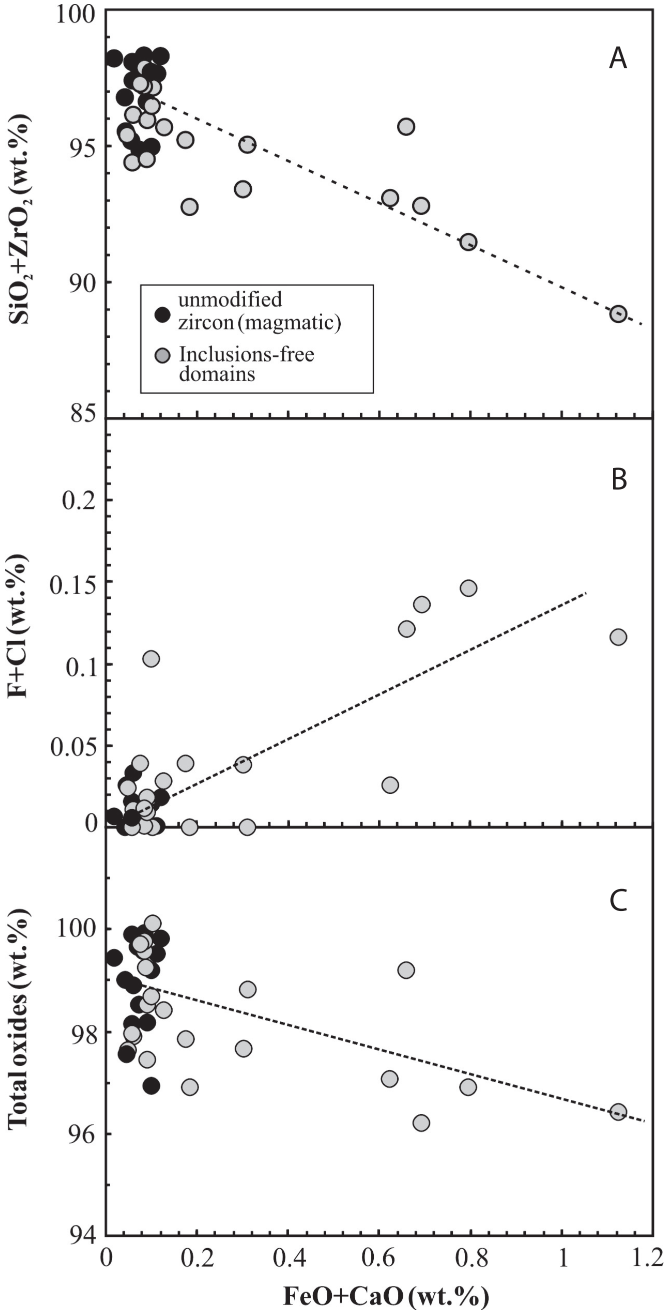

Fig. 12. Bi-modal plots of FeO+CaO vs. SiO_2+ZrO_2 (A), F+Cl (B), and total oxides (C). It is notable that FeO+CaO are negatively correlated with SiO_2+ZrO_2 and total oxides but positively correlated with F+Cl (A, B), suggesting that in addition to Ca, Al, and Fe, the F, Cl, and/or OH may also diffuse from the fluids into the zircon, whereas Zr and Si from the magmatic zircon are lost to the fluids. See the text for more details.

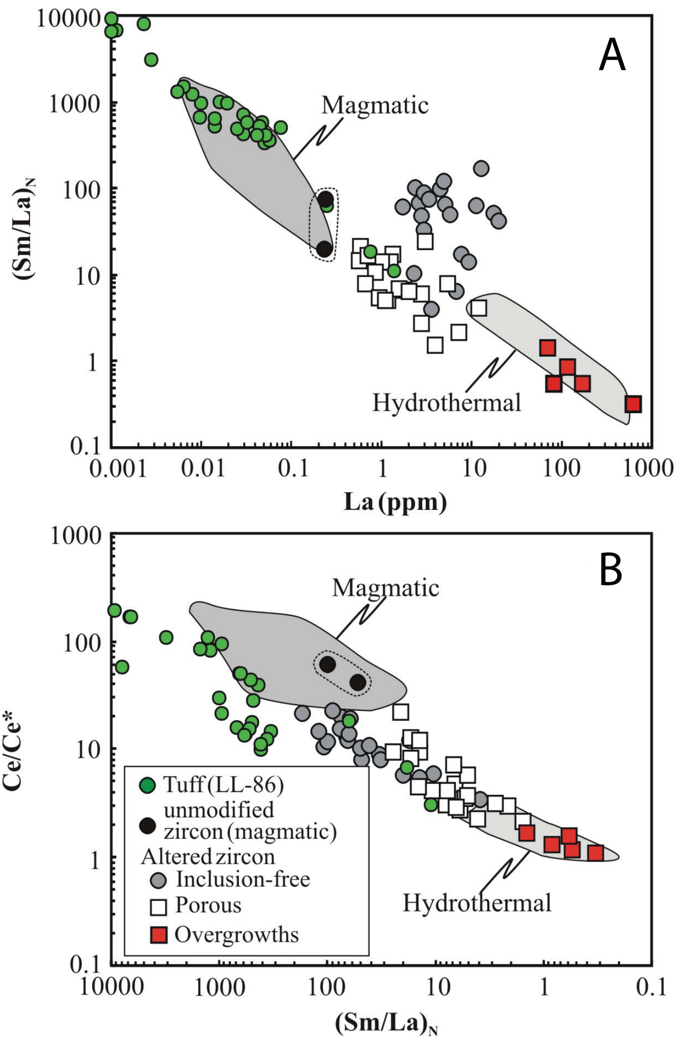

Fig. 13. Discrimination diagrams of different types of zircon or domains. Analyses of the overgrowth/rims are all plotted in the 'hydrothermal zircon' field, whereas those of the unmodified (magmatic) zircon are plotted close to the 'magmatic' field. Note that the inclusion-free and porous domains are plotted in the places between the 'hydrothermal' and 'magmatic' fields. Both (A) and (B) are modified from Hoskin (2005).

tion, and act as "non-formula" elements (Hoskin and others, 2000; Hoskin and Schaltegger, 2003). Thus, these elements cannot be incorporated into structures of typical magmatic zircon. Instead, they are able to diffuse from fluids to zircon through diffusion-reaction process during zircon-fluid interaction, and were finally dissolved as the form of nano-sized amorphous remnants in the zircon hosts (Geisler and others, 2003, 2007). As such, we conclude that the inclusion-free domains were products of interaction between magmatic zircon and fluids through the so-called diffusion-reaction process. It is notable that the total FeO + CaO contents are negatively correlated with total SiO_2+ZrO_2 but positively correlated with total F+Cl (figs. 12A and 12B). This implies that, in addition to Ca, Al, and Fe, both F and Cl may have also diffused into the zircon grains, whereas Zr and Si from the magmatic zircon have been lost to the fluids. There is also a negative correlation between the total oxides and total FeO+CaO (fig. 12c), indicating that other non-analyzed elements (most likely OH) also migrated into the zircon by diffusion (Geisler and others, 2007).

Formation of the porous domains via dissolution-reprecipitation.—The textural relationships show that in many cases, the porous domains penetrate the inclusion-free domains (fig. 4), indicating that the porous domains are likely slightly older than or simultaneous with the inclusion-free domains (fig. 14) (compare Rubatto and others, 2008). The morphology and porous appearances of the porous domains are quite similar to those modified by metamorphic fluids (for example Corfu and others, 2003; Hoskin and Schaltegger, 2003; Tomaschek and others, 2003; Rubatto and others, 2008; Taylor and others, 2014). Formation of such porous zircon domains is commonly thought to involve a dissolution-reprecipitation process in the presence of fluid phases (Putnis, 2002; Tomaschek and others, 2003; Rubatto and others, 2008; Martin and others, 2008; Hay and Dempster, 2009). It is generally considered that the dissolution-reprecipitation process would involve breaking of bonds and release of elements (that is dissolution), accompanied by contemporaneous nucleation and growth (that is reprecipitation) of new, relatively "pure" zircon (depleted in trace elements) and trace element-rich phases (for example, Th, HREE or Y-rich phases), at an inward-moving interface (Tomaschek and others, 2003; Geisler and others, 2007). In our case, it is clearly shown that the porous domains contain abundant fine-grained, single-phase inclusions of (HREE-Y)-rich silicates (likely thalenite), thorite, or xenotime (figs. 5 and 6), thus consistent with their formation through a dissolution-reprecipitation process. This interpretation is further supported by the fact that compared to the precursor, inclusion-free domains or magmatic zircon, the porous domains do have much lower Y, P, REE, and Th contents (figs. 7B, 8, 9A, and 9B).

Other than containing the inclusions of (HREE-Y)-rich silicates, thorite and xenotime that are solely sourced from the original zircon hosts, some porous domains contain abundant pores or inclusions of hydrothermal minerals, albite, actinolite, calcite, and chlorite, that totally have more than 20 volume percent of the hosts (figs. 5A, 5B and 6). These hydrothermal minerals cannot be sourced from the zircon hosts but external fluids, thus implying that the dissolved components of zircon were partially transported out of the hosts by the external fluid, a process that is likely due to high solubility of zircon in such a fluid or under-saturation of the fluid with respect to Zr or Si.

Precipitation of the rims from the external fluids.—The rims have low concentrations of "non-formula" elements (fig. 6C; Appendix fig. A1) and pronounced enrichments of LREEs contents with low $(Sm/La)_N$ and Ce/Ce* ratios (figs. 9C, 9D and 10), similar to those of typical hydrothermal zircon precipitated from fluids (figs. 14A and 14B) (Hoskin, 2005). Although it is possible that the Zr in the fluids precipitating the rims were sourced from the dissolved components of the zircon hosts as indicated above by the large volumes of pores or voids, the precipitation of the rims in this study was not related to the documented dissolution-reprecipitation process in which dissolution and reprecipitation are temporally and spatially connected (Ayers and others, 2003; Geisler and others, 2007). Indeed, these rims are generally homogeneous under BSE imaging, and do not contain any single-phase inclusions of (HREE-Y)-rich silicates, thorite, or xenotime that are expected to be formed in a dissolution-reprecipitation process. Moreover, the rims are characterized by distinctly high LREE and Hf isotopic ratios relative to the porous domains (figs. 9C and 11), supporting the conclusion that the chemical components responsible for the formation of the rims cannot solely come from the parental grain but were also partially provided by external fluids.

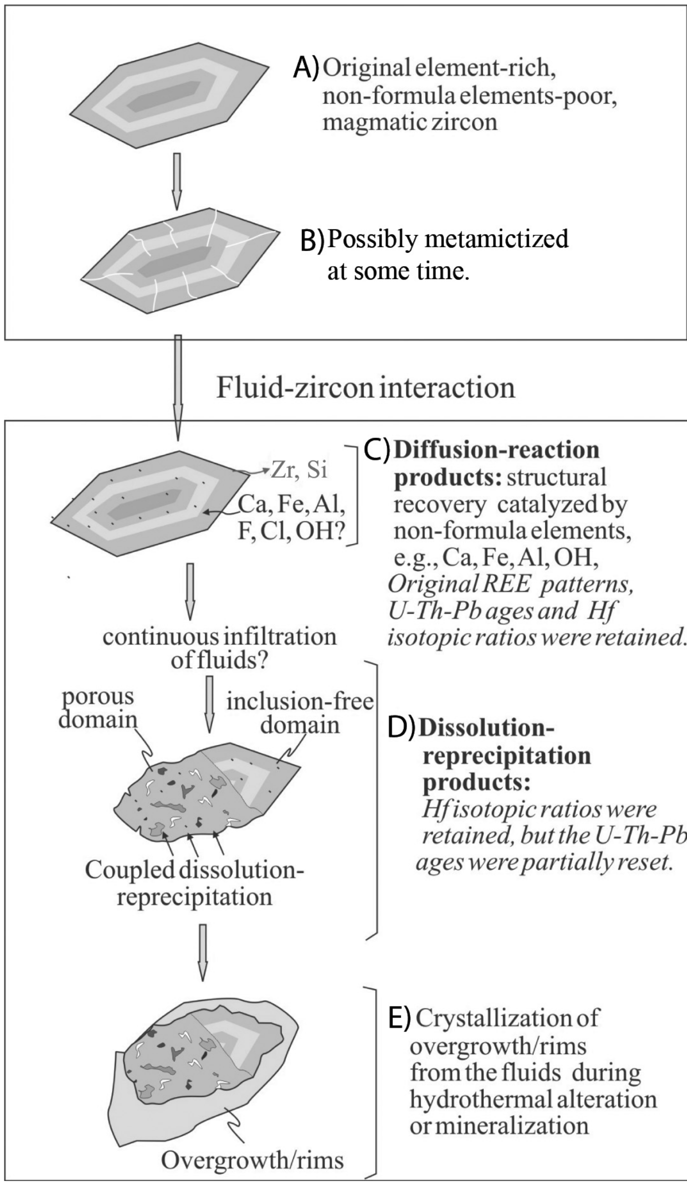

Fig. 14. A schematic diagram showing the formation of different domains and overgrowth/rims of altered zircon from the gabbros. The altered zircon originates from primary Th-U-rich magmatic zircon (A), and was likely metamictized at some time before alteration (B). Alteration of the metamict zircon followed a sequence of an early diffusion-reaction process forming the inclusion-free domains (C), followed by the dissolution-reprecipitation process forming the porous domains (D). The overgrowth/rims were the last to have crystallized, surrounding the inclusion-free or porous domains (E). Details are referred to in the text.

Possible Controls on Hydrothermal Alteration of Zircon

Primary plagioclase and clinopyroxene from the host gabbros are completely replaced by hydrothermal mineral assemblages of both the early Fe mineralization stage accompanied with Na-Fe alteration, including albite, magnetite, chlorite, and actinolite, and the late Cu mineralization stage accompanied with K-carbonate alteration, including K-feldspar, calcite, and biotite (Chen and Zhou, 2012, 2015). Similarly, inclusions in the altered zircon and the surrounding matrix have a similar assemblage that refers to the minerals present in both the Fe and Cu mineralization stages, indicating that the alteration of magmatic zircon is genetically related to both the Fe and Cu mineralizing fluids. Previous studies of fluid inclusion and mineral chemistry indicate that the Fe mineralizing fluids have high salinity (up to 36 equiv. wt% NaCl) with temperatures ranging of 375 to 460 °C (Shentu, 1997; Jin and Shen, 1998), whereas the Cu mineralizing fluids have much lower salinity (13–17 wt% NaCl) and temperatures (230–400 °C) but higher pH values, K/Na and F/Cl ratios, and Ca concentrations (Yu and Liu, 1988; Sun and Liu, 1990; Chen and others, 1991; Shentu, 1997; Jin and Shen, 1998; Chen and Zhou, 2015). These results indicate that the magmatic zircon in the gabbros was essentially modified by NaCl-dominant fluids with variable temperature, pressure and pH, and concentrations of F, Ca and K (Chen and Zhou, 2015). In other words, the magmatic zircon in the gabbros is able to be modified by NaCl-rich brines, but effects of fluid salinity, temperature, pH, pressure or variable Fe, Ca and K on the alteration of zircon tend to be unremarkable.

It is noteworthy to mention that the zircon grains from an altered tuff sample in the Lala mine are all primary and magmatic and do not show any signs of modification or alteration (Chen and others, 2013). They are mostly euhedral with clear oscillatory growth zoning (fig. 8A), and have extremely low concentrations of "non-formula" elements (for example, Ca<200 ppm; Al mostly <10 ppm) similar to those of typical magmatic zircon (Appendix table A2; figs. 6C, 9A, 13A, and 13B). Such a good preservation of magmatic zircon in altered tuffs from the same mine clearly suggests that the original, magmatic zircon grains were resistant to the NaCl-dominant fluids that modified the magmatic zircon from the gabbros. The different responses of zircon to the fluids thus allow us to propose that in addition to the presence of the NaCl-rich brines, the nature of the precursor, magmatic zircon (for example, trace-element budgets or metamictization; Geisler and others, 2007) should also be an important control on the hydrothermal modification of zircon in the gabbros. Indeed, it was considered that in a fluid-zircon solid solution (that is $ZrSiO_4$-$MSiO_4$; "M" represents Th or U) interaction system, the zircon solid solution with higher components of $MSiO_4$ have a higher solubility in an aqueous liquid than the pure zircon end-member (Lippmann, 1980; Geisler and others, 2007). In other words, $MSiO_4$-rich zircon is highly reactive to the fluids relative to $MSiO_4$-poor zircon (Geisler and others, 2007). Indeed, magmatic zircon from the tuff does have much lower REE, Y, P, Th (41–289 ppm; mostly <120 ppm), and U (62–300 ppm; mostly <150 ppm) concentrations than that of the gabbros (Appendix table A2; for example, fig. 8B), and it is noteworthy that several survived magmatic zircon grains in the altered gabbros do have lowest Th and U (or REE, Y, P) concentrations (figs. 8A, 8B and 9A). Therefore, we conclude that the relatively high solubility for the element-rich, magmatic zircon in the gabbros is likely one of the important factors for enhancing alteration of zircon.

The Th-U-rich magmatic zircon in the gabbros should be also more susceptible to radiation damage (that is metamictization) than the relatively "compositionally pure" zircon in the tuffs, due to the decay of Th and U. Metamictization is able to cause swellings of amorphous areas, generating a series of fractures (Hay and Dempster, 2009), thus increasing the reactivity of zircon to the fluids (Murakami and others, 1991; Geisler and others, 2003, 2005; Ewing and others, 2003; Wang and others, 2014; McGloin and others, 2015). In our case, most of the altered zircon, particularly the Th-U-rich inclusion-free domains, do have radial cracks or fractures (figs. 4C, 5G, and 5H), suggesting that high Th and U, and the resultant metamictization, can be important controls enhancing hydrothermal alteration of the zircon. It is also noteworthy that some Th-U-rich inclusion-free domains do not have clear fractures or cracks (figs. 5A, 5B, and 5F). However, we cannot exclude the possibility that the precursors of these domains may have once been metamictized before alteration (figs. 14B and 14C), as metamictized, magmatic zircon can be structurally recovered or revamped by diffusion of "non-formula" elements such as Ca, Fe, Al, OH, F, and Cl, through the diffusion-reaction process (Geisler and others, 2003, 2005, 2007; Martin and others, 2008).

Implications

This study demonstrates that NaCl-bearing brines are capable to modify zircon, and that the nature of the precursor, magmatic zircon (for example, composition or metamictization) are a prerequisite for hydrothermal modification. Given that NaCl-rich brines are very common in many hydrothermal systems, we speculate that alteration of Th-U-rich zircon should be ubiquitous in altered rocks adjacent to hydrothermal deposits. However, as will be discussed below, even if the primary magmatic zircon was partially or completely modified, its altered products may still potentially record the timing or nature of multiple tectonothermal or hydrothermal events, particularly the ages of metamorphism or mineralization, which are in many cases very difficult to determine (Pelleter and others, 2007; Fu and others, 2009).

It was considered that interaction between zircon and fluids via a diffusion-reaction process likely results in the loss of Zr, Si, Hf, REE, U, Th, and radiogenic Pb from the precursor zircon (Sinha and others, 1992; Geisler and others, 2003, 2007; Martin and others, 2008). In addition, common Pb was suggested to likely diffuse to the zircon hosts, and dissolved in some nano-sized, secondary phases during the interaction, thus variably modifying the original U-Pb system. However, in our case that involved low-temperature, NaCl-rich brines, such kinds of modifications on element and isotopic systems are not observed in the inclusion-free domains that were formed via the diffusion-reaction process. Instead, except the elevated Ca, Fe, and Al (fig. 12), the inclusion-free domains almost retained the same REE patterns, Th and U concentrations, U-Pb ages, and Hf isotopic ratios of the precursor, magmatic zircon (figs. 8, 9, 10A, and 11).

On the other hand, a dissolution-reprecipitation process resulted in precipitation of new zircon, and thus the porous domains formed in this way are expected to have similarly reset, meaningful U-Pb ages and Hf isotopic ratios as those from some metamorphic or hydrothermally modified rocks (for example, Martin and others, 2008; Campbell and others, 2014; Van Lankvelt and others, 2016). However, our new results illustrate that the porous domains retained the Hf isotopic ratios of the inclusion-free domains or magmatic zircon (figs. 6B and 11), but exhibit a wide range of discordant $^{207}Pb/^{206}Pb$ apparent ages (Appendix tables A3 and A4; fig. 10B) with considerable amounts of common Pb (Appendix fig. 2). This feature indicates that the U-Pb and Lu-Hf isotopic systems are decoupled during formation of the porous domains. It seems that initial Hf isotopic ratios once "set" in the magmatic zircon structure remains nearly unaffected during hydrothermal alteration (for example, Gerdes and Zeh, 2009). In contrast, the variable and discordant U-Pb ages for the porous domains provide a strong hint that the U-Pb system was variably modified but not completely reset. These unusual behaviors of U-Pb systems during alteration are likely explained as: 1) Pb loss after the formation of the porous domains, 2) protracted formation of the porous domains, 3) accidental ablation of visible or invisible mineral inclusions during measurement as revealed by their high Ca, Fe and Al concentrations (fig. 6C). The first explanation can be ruled out because the U-Pb analyses do not form a clear Pb-loss regression line (fig. 9B). A protracted hydrothermal event is also not evident in this region (Zhou and others, 2014). Accidental ablation of mineral inclusions is possible, particularly for those analyses with high common Pb that is responsible for the unreasonably high $^{207}Pb/^{206}Pb$ apparent ages without common Pb correction (Appendix table A3). However, ablation of visible mineral inclusions can be ruled out, as the measurement was well monitored by time-resolved signal variations, and most of the analyses for the porous domains containing common Pb do not show any signs of accidental contamination related to some visible inclusions (for example, stable Pb, Fe, Al, or Ca time-resolved signals; Appendix fig. A2). We propose that the most possible explanation for the stable Fe, Al, or Ca signals should be due to the presence of invisible, nano-sized Ca-Al-Fe-rich phases that are likely homogeneously distributed in the porous domains. Regarding the origin of such kind of Ca-Al-Fe-rich phases in the porous domains, the possibility that they were "inherited" from those present in the early inclusion-free domains can be reasonably ruled out, because the inclusion-free domains do not contain any considerable amounts of common Pb that generally cannot be incorporated into zircon structure. Alternatively, the Ca-Al-Fe-rich phases with common Pb may have precipitated from the external fluids, together with newly crystallized zircon during the dissolution-reprecipitation process. Therefore, the U-Pb ages and $^{176}Hf/^{177}Hf$ ratios of the porous domains are meaningless and cannot be used to constrain ages of possible hydrothermal/mineralization events. Instead, the timing of the event is well recorded in the locally present rims (fig. 10C), which have a robust U-Pb age within error to the molybdenite Re-Os and allanite U-Pb ages of the Lala deposit (~1.07 Ga) (Chen and Zhou, 2012, 2014).

In summary, even though alteration mechanism of zircon under metamorphic conditions was previously well constrained, our study clearly indicates that the magmatic zircon may have acted differently in the presence of a NaCl-rich brine that is very common in many hydrothermal deposits. Our work may thus also shed some light on further experimental studies concerning alteration of different zircon related to NaCl-rich fluids under low-temperature hydrothermal conditions.

CONCLUSIONS

This study illustrates that alteration of magmatic zircon grains related to low-temperature, NaCl-rich fluids involved both diffusion-reaction and dissolution-reprecipitation processes. In addition to the presence of NaCl-rich fluids, high Th and U contents and/or resultant metamictization of zircon grains are likely important controls on the alteration of zircon. The diffusion-reaction process is able to revamp the metamict precursor zircon to form the so-called inclusion-free domains that retained almost all the magmatic features (for example, Th and U contents, REE patterns, U-Pb age and Hf isotope) of the precursors. Continuous hydrothermal modification of the inclusion-free domains or magmatic zircon through a dissolution-reprecipitation process has produced the porous domains, which involved reprecipitation of new, trace element-poor zircon together with abundant inclusions of fine-grained Y-HREE-Th-rich phases. The porous domains retained the Hf isotopic ratios of the precursor, inclusion-free domains or magmatic zircon, but exhibit a wide range of discordant $^{207}Pb/^{206}Pb$ apparent ages without clear geological meanings. This unusual feature was possibly attributed to the presence of invisible, nano-sized Ca-Fe-Al-rich phases that have co-precipitated with the newly crystallized zircon during the dissolution-reprecipitation process. Instead, a meaningful U-Pb age is well recorded in the rims over the altered zircon, representing the timing of the Fe-Cu mineralization. As NaCl-rich brines are very common in many hydrothermal systems, we highlight that alteration of Th-U-rich zircon should be ubiquitous in altered rocks adjacent to hydrothermal deposits. However, we also suggest that a clear understanding of the complex textures of hydrothermally modified zircons can provide important information about the origin and timing of multiple tectonothermal, hydrothermal, or mineralization events.

ACKNOWLEDGMENTS

This study is supported by grants from the National Natural Science Foundation of China (Grant 41673048 and 41272212) and Key Research Program of Frontier Sciences, CAS (QYZDB-SSW-DQC008). Additional support was provided by the "Thousand Youth Talents

Plan" grant to Wei Terry Chen. We thank geologists from the Lala Mine, especially Mr. Liang Chen and Dinghua Ma for their help during the field work. Mrs Chen Linli, Dr. Xianglin Tu, Jean Wong, and Helen Geng are greatly appreciated for their assistance with the analyses. Special thanks are due to Professor Julian Pearce for providing constructive suggestions on an early draft of the manuscript. We are grateful to the official reviews by Callum Hetherington and Daniel Harlov, and editorial handling by Ethan Baxter.

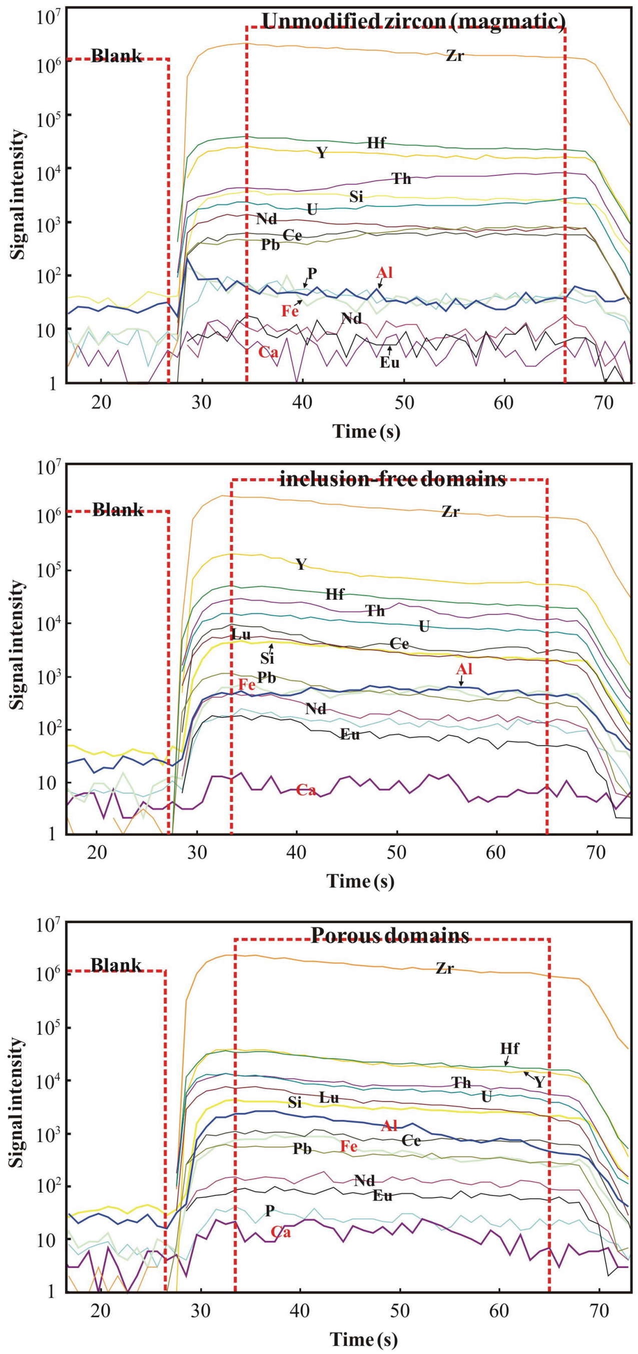

Fig. A1. LA-ICPMS time-resolved signal diagram of trace elements of zircon. It is clear that both the inclusion-free and porous domains contain considerable Ca, Al and Fe (stable signals).

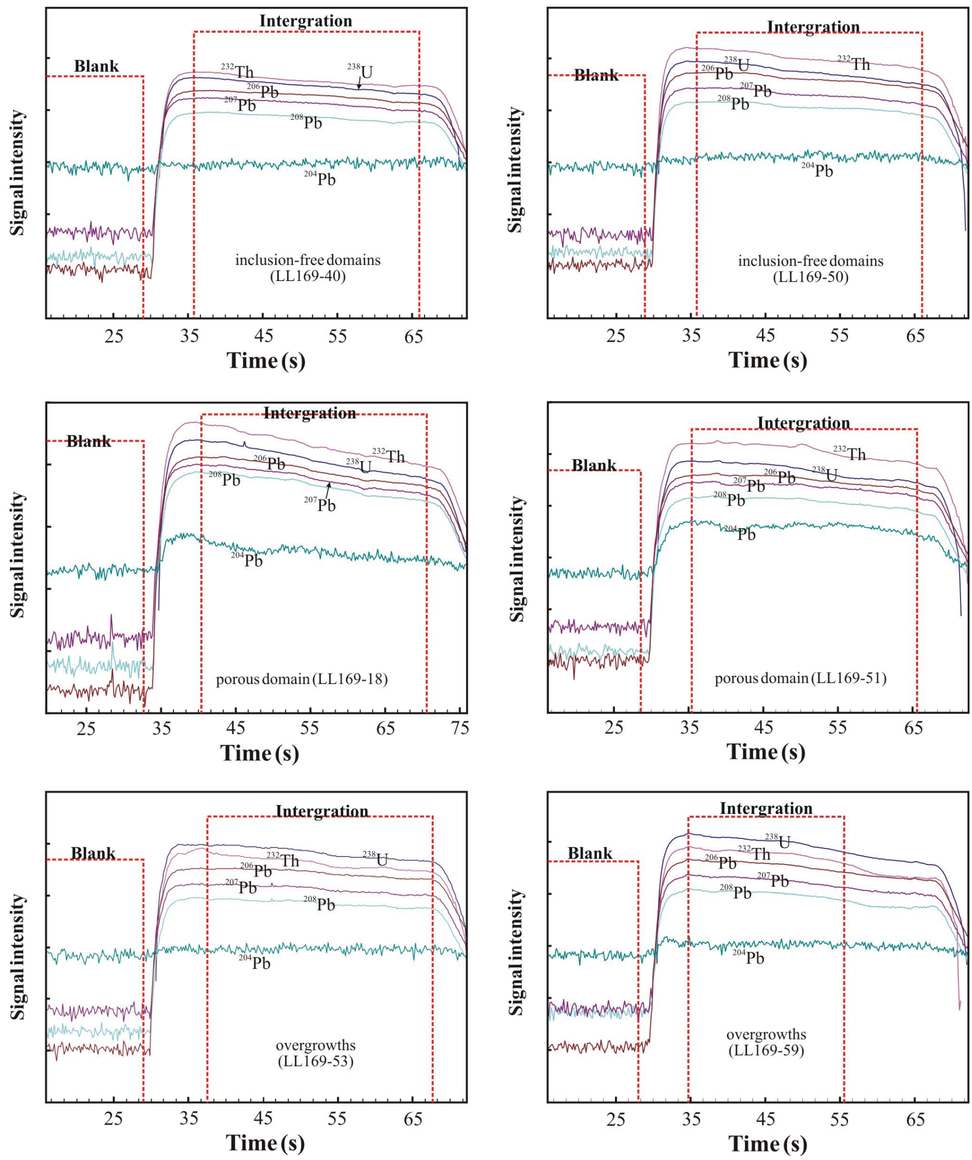

Fig. A2. LA-MC-ICPMS time-resolved signal diagram of U-Th-Pb ages of zircon. It is notable that the porous domains contain considerable common Pb (stable Pb204 signal), whereas the common Pb in the inclusion-free domains and overgrowths is negligible.

Table A1

Electron microprobe analyses of zircon from altered gabbros

Element	Unmodified, magmatic zircon									
wt%	LL169-1-13	LL169-1-14	LL169-1-21	LL169-1-25	LL169-1-26	LL169-1-27	LL169-1-35	LL169-2-12	LL169-2-13	LL169-2-19
SiO_2	33.05	32.77	33.61	33.45	33.38	33.99	33.79	33.62	33.69	33.34
ZrO_2	62.49	62.20	64.60	63.95	61.48	62.64	64.50	64.12	64.03	63.44
HfO_2	1.37	1.28	1.20	1.37	1.32	1.43	1.36	1.42	1.30	1.47
ThO_2	0.44	0.09	b.d.	0.05	0.67	0.03	b.d.	0.25	b.d.	0.21
Y_2O_3	0.14	0.48	b.d.	b.d.	1.61	b.d.	0.03	0.08	0.08	0.50
P_2O_5	b.d.	0.00	b.d.	b.d.	b.d.	b.d.	b.d.	b.d.	b.d.	b.d.
FeO	b.d.	0.06	b.d.	0.04	0.04	0.05	0.06	0.06	0.08	0.02
CaO	0.03	0.04	b.d.	b.d.	0.04	0.04	0.06	b.d.	b.d.	0.03
F	b.d.	b.d.	b.d.	0.03	b.d.	b.d.	b.d.	b.d.	b.d.	b.d.
Cl	0.03	b.d.	b.d.	b.d.	b.d.	b.d.	b.d.	b.d.	b.d.	b.d.
-O=F,Cl	b.d.	b.d.	b.d.	b.d.	b.d.	b.d.	b.d.	b.d.	b.d.	b.d.
total	97.55	96.93	99.43	98.91	98.54	98.18	99.82	99.59	99.21	99.00
Element	**Unmodified, magmatic zircon**					**Inclusion-free domains**				
wt%	LL169-2-10	LL169-2-22	LL169-2-26	LL169-2-27	LL169-2-42	LL169-1-5	LL169-1-4	LL169-1-11	LL169-1-9	LL169-1-15
SiO_2	33.81	33.02	34.15	33.64	33.40	32.78	33.60	33.05	33.51	32.36
ZrO_2	63.85	62.17	64.17	64.44	64.53	62.27	63.55	62.66	64.13	60.45
HfO_2	1.35	1.44	1.51	1.62	1.26	1.32	1.22	1.36	1.26	1.20
ThO_2	0.29	0.48	0.00	0.12	0.34	0.89	1.06	1.18	0.27	0.57
Y_2O_3	0.11	0.96	0.00	0.00	0.04	1.26	0.58	0.20	0.00	0.84
P_2O_5	b.d.	b.d.	b.d.	b.d.	b.d.	b.d.	b.d.	b.d.	b.d.	b.d.
FeO	0.10	b.d.	0.07	0.04	0.04	0.30	0.08	0.51	0.06	0.54
CaO	b.d.	0.04	b.d.	b.d.	b.d.	b.d.	b.d.	0.15	b.d.	0.15
F	b.d.	b.d.	b.d.	b.d.	b.d.	b.d.	b.d.	b.d.	b.d.	b.d.
Cl	b.d.	0.02	b.d.	0.01	0.01	b.d.	b.d.	0.12	b.d.	0.14
-O=F,Cl	b.d.	b.d.	b.d.	b.d.	b.d.	b.d.	b.d.	b.d.	b.d.	b.d.
total	99.52	98.14	99.92	99.89	99.66	98.83	100.12	99.19	99.26	96.22
Element	**Inclusion-free domains**									
wt%	LL169-1-16	LL169-1-18	LL169-1-28	LL169-1-31	LL169-1-37	LL169-1-38	LL169-1-50	LL169-1-52	LL169-2-5	LL169-2-6
SiO_2	31.75	32.88	33.57	33.51	33.20	33.25	33.33	33.12	32.99	32.66
ZrO_2	59.73	63.26	64.30	61.90	62.75	61.15	62.35	62.10	63.48	60.43
HfO_2	1.32	1.41	1.47	1.34	1.23	1.48	1.32	1.47	1.40	1.35
ThO_2	1.63	0.29	0.14	0.36	0.57	0.47	0.67	0.54	0.20	1.22
Y_2O_3	1.58	b.d.	b.d.	0.46	0.68	1.54	0.59	0.43	0.43	0.78
P_2O_5	b.d.	b.d.	b.d.	b.d.	b.d.	b.d.	b.d.	b.d.	b.d.	b.d.
FeO	0.58	0.03	0.06	b.d.	0.08	0.04	0.10	0.12	0.07	0.46
CaO	0.22	0.03	0.03	0.03	b.d.	b.d.	0.03	0.05	0.03	0.16
F	b.d.	b.d.	b.d.	b.d.	b.d.	b.d.	b.d.	b.d.	b.d.	b.d.
Cl	0.14	b.d.	b.d.	b.d.	b.d.	b.d.	0.03	0.04	0.10	0.03
-O=F,Cl	b.d.	b.d.	b.d.	b.d.	b.d.	b.d.	b.d.	b.d.	b.d.	b.d.
total	96.91	97.90	99.57	97.62	98.52	97.95	98.41	97.86	98.69	97.08
Element	**Inclusion-free domains**						**Porous domains**			
wt%	LL169-2-21	LL169-2-15	LL169-2-35	LL169-2-43	LL169-2-39	LL169-2-29	LL169-1-1	LL169-1-2	LL169-1-6	LL169-1-7
SiO_2	33.23	33.48	34.02	32.81	33.95	32.17	33.78	34.24	33.05	33.46
ZrO_2	60.18	61.04	63.17	59.95	63.33	56.67	64.70	64.43	62.69	65.07
HfO_2	1.61	1.41	1.34	1.32	1.49	1.28	1.31	1.23	1.71	1.69
ThO_2	1.11	0.53	0.82	0.62	0.35	2.03	0.04	0.18	b.d.	b.d.
Y_2O_3	1.20	0.89	0.32	2.02	0.47	2.84	b.d.	b.d.	0.26	b.d.
P_2O_5	b.d.	b.d.	b.d.	b.d.	b.d.	0.23	b.d.	b.d.	b.d.	b.d.
FeO	0.21	0.07	0.08	0.15	0.04	0.76	0.09	0.09	0.09	0.05
CaO	0.09	b.d.	b.d.	0.04	0.04	0.36	b.d.	0.03	b.d.	0.04
F	b.d.	b.d.	b.d.	b.d.	b.d.	b.d.	b.d.	b.d.	b.d.	b.d.
Cl	0.04	b.d.	b.d.	b.d.	b.d.	0.12	b.d.	b.d.	b.d.	b.d.
-O=F,Cl	b.d.	b.d.	b.d.	b.d.	b.d.	b.d.	b.d.	b.d.	b.d.	b.d.
total	97.67	97.45	99.76	96.90	99.70	96.43	99.96	100.20	97.84	100.33

Table A1
(continued)

Element	Porous domains									
wt%	LL169-1-8	LL169-1-10	LL169-1-12	LL169-1-17	LL169-1-19	LL169-1-20	LL169-1-22	LL169-1-23	LL169-1-24	LL169-1-29
SiO_2	33.19	33.19	33.11	32.88	32.91	33.56	33.08	33.45	32.88	32.69
ZrO_2	60.81	65.43	63.08	61.58	62.55	63.04	61.34	63.76	62.78	62.52
HfO_2	1.26	1.31	1.40	1.53	1.68	1.54	1.28	1.67	1.39	1.13
ThO_2	0.24	b.d.	0.19	0.27	0.25	0.60	0.14	0.01	0.29	b.d.
Y_2O_3	0.94	b.d.	0.21	0.58	b.d.	b.d.	b.d.	b.d.	0.28	0.25
P_2O_5	b.d.	b.d.	b.d.	b.d.	b.d.	b.d.	b.d.	b.d.	b.d.	b.d.
FeO	0.34	0.06	0.09	0.07	0.33	0.14	0.28	0.04	0.11	0.13
CaO	0.12	b.d.	0.08	0.06	0.06	0.03	0.21	0.03	0.03	0.04
F	b.d.	b.d.	b.d.	b.d.	b.d.	b.d.	b.d.	b.d.	b.d.	b.d.
Cl	0.08	0.03	0.55	0.05	0.34	b.d.	0.04	b.d.	0.07	0.05
-O=F,Cl	b.d.	b.d.	b.d.	b.d.	b.d.	b.d.	b.d.	b.d.	b.d.	b.d.
total	96.96	100.03	98.59	97.01	98.05	98.95	96.34	98.99	97.83	96.79

Element	Porous domains									
wt%	LL169-1-30	LL169-1-32	LL169-1-33	LL169-1-34	LL169-1-39	LL169-1-40	LL169-1-43	LL169-1-44	LL169-1-46	LL169-1-48
SiO_2	33.70	33.43	33.63	33.29	33.71	33.86	33.71	32.35	32.93	33.81
ZrO_2	63.54	63.07	64.39	60.67	62.66	63.60	63.92	61.25	60.75	64.08
HfO_2	1.37	1.58	1.48	1.47	1.64	1.35	1.47	1.38	1.25	1.53
ThO_2	0.29	0.27	0.21	1.86	0.92	0.52	0.13	0.51	0.48	0.04
Y_2O_3	b.d.	0.34	b.d.	0.57	0.70	0.47	0.34	0.57	1.36	b.d.
P_2O_5	b.d.	b.d.	b.d.	b.d.	b.d.	b.d.	b.d.	b.d.	b.d.	b.d.
FeO	0.11	0.10	0.10	0.77	0.08	0.11	0.07	0.42	0.05	b.d.
CaO	0.04	0.03	b.d.	0.31	0.04	b.d.	b.d.	0.07	0.04	0.04
F	b.d.	b.d.	b.d.	b.d.	b.d.	b.d.	b.d.	b.d.	b.d.	b.d.
Cl	b.d.	b.d.	b.d.	0.07	0.07	b.d.	b.d.	0.05	0.06	b.d.
-O=F,Cl	b.d.	b.d.	b.d.	b.d.	b.d.	b.d.	b.d.	b.d.	b.d.	b.d.
total	99.05	98.83	99.85	98.99	99.80	99.94	99.65	96.58	96.90	99.51

Element	Porous domains									
wt%	LL169-1-49	LL169-1-51	LL169-1-53	LL169-2-1	LL169-2-3	LL169-2-4	LL169-2-7	LL169-2-9	LL169-2-11	LL169-2-14
SiO_2	33.51	32.14	33.08	33.10	33.00	33.53	33.13	32.03	33.11	31.80
ZrO_2	62.07	57.52	64.76	61.60	56.94	62.84	62.82	58.78	62.62	57.46
HfO_2	1.53	1.52	1.49	1.57	1.42	1.51	1.56	1.29	1.66	1.30
ThO_2	b.d.	0.34	0.19	0.53	1.01	0.20	0.47	1.20	0.19	0.59
Y_2O_3	0.13	0.03	0.04	0.57	3.92	0.03	0.00	1.76	0.07	2.69
P_2O_5	b.d.	b.d.	b.d.	b.d.	b.d.	b.d.	b.d.	b.d.	b.d.	b.d.
FeO	0.08	0.80	0.12	0.37	0.23	0.08	0.15	0.60	0.21	0.33
CaO	0.03	0.06	0.03	0.14	0.07	0.05	0.13	0.19	0.11	0.05
F	b.d.	b.d.	b.d.	b.d.	b.d.	0.04	b.d.	b.d.	b.d.	b.d.
Cl	0.03	0.05	0.03	0.09	0.08	0.03	0.05	0.12	0.16	b.d.
-O=F,Cl	b.d.	b.d.	b.d.	b.d.	b.d.	0.02	b.d.	b.d.	b.d.	b.d.
total	97.37	92.43	99.74	97.96	96.64	98.29	98.29	95.94	98.11	94.23

Element	Porous domains											
wt%	LL169-2-16	LL169-2-17	LL169-2-20	LL169-2-23	LL169-2-24		LL169-2-25		LL169-2-31	LL169-2-32	LL169-2-33	LL169-2-34
SiO_2	32.91	32.99	33.51	33.74	32.81		33.40		33.31	33.09	33.26	33.68
ZrO_2	63.37	59.99	63.87	63.66	59.83		64.70		61.65	62.30	64.74	64.44
HfO_2	1.41	1.35	1.42	1.58	1.41		1.67		1.46	1.43	1.71	1.35
ThO_2	0.25	0.70	0.41	0.15	0.53		0.21		0.98	0.28	b.d.	0.38
Y_2O_3	0.15	2.32	0.60	b.d.	2.77		b.d.		0.38	0.94	b.d.	b.d.
P_2O_5	b.d.	0.07	0.00	b.d.	0.07		b.d.		b.d.	b.d.	b.d.	b.d.
FeO	0.11	0.05	0.13	b.d.	0.05		0.09		0.55	0.03	0.09	0.06
CaO	0.04	b.d.	0.03	0.06	0.03		0.03		0.15	0.02	0.03	0.05
F	b.d.	b.d.	b.d.	b.d.	b.d.		b.d.		b.d.	b.d.	b.d.	b.d.
Cl	0.12	b.d.	b.d.	0.04	b.d.		0.05		0.08	0.04	b.d.	0.11
-O=F,Cl	b.d.	b.d.	b.d.	b.d.	b.d.	b.d.	b.d.	b.d.	b.d.	b.d.	b.d.	b.d.
total	98.34	97.48	99.98	99.23	97.51		100.14		98.54	98.11	99.83	100.07

Table A1

(continued)

Element	Porous domains									
wt%	LL169-1-49	LL169-1-51	LL169-1-53	LL169-2-1	LL169-2-3	LL169-2-4	LL169-2-7	LL169-2-9	LL169-2-11	LL169-2-14
SiO_2	33.51	32.14	33.08	33.10	33.00	33.53	33.13	32.03	33.11	31.80
ZrO_2	62.07	57.52	64.76	61.60	56.94	62.84	62.82	58.78	62.62	57.46
HfO_2	1.53	1.52	1.49	1.57	1.42	1.51	1.56	1.29	1.66	1.30
ThO_2	b.d.	0.34	0.19	0.53	1.01	0.20	0.47	1.20	0.19	0.59
Y_2O_3	0.13	0.03	0.04	0.57	3.92	0.03	0.00	1.76	0.07	2.69
P_2O_5	b.d.	b.d.	b.d.	b.d.	b.d.	b.d.	b.d.	b.d.	b.d.	b.d.
FeO	0.08	0.80	0.12	0.37	0.23	0.08	0.15	0.60	0.21	0.33
CaO	0.03	0.06	0.03	0.14	0.07	0.05	0.13	0.19	0.11	0.05
F	b.d.	b.d.	b.d.	b.d.	b.d.	0.04	b.d.	b.d.	b.d.	b.d.
Cl	0.03	0.05	0.03	0.09	0.08	0.03	0.05	0.12	0.16	b.d.
-O=F,Cl	b.d.	b.d.	b.d.	b.d.	b.d.	0.02	b.d.	b.d.	b.d.	b.d.
total	97.37	92.43	99.74	97.96	96.64	98.29	98.29	95.94	98.11	94.23

Element	Porous domains									
wt%	LL169-2-16	LL169-2-17	LL169-2-20	LL169-2-23	LL169-2-24	LL169-2-25	LL169-2-31	LL169-2-32	LL169-2-33	LL169-2-34
SiO_2	32.91	32.99	33.51	33.74	32.81	33.40	33.31	33.09	33.26	33.68
ZrO_2	63.37	59.99	63.87	63.66	59.83	64.70	61.65	62.30	64.74	64.44
HfO_2	1.41	1.35	1.42	1.58	1.41	1.67	1.46	1.43	1.71	1.35
ThO_2	0.25	0.70	0.41	0.15	0.53	0.21	0.98	0.28	b.d.	0.38
Y_2O_3	0.15	2.32	0.60	b.d.	2.77	b.d.	0.38	0.94	b.d.	b.d.
P_2O_5	b.d.	0.07	0.00	b.d.	0.07	b.d.	b.d.	b.d.	b.d.	b.d.
FeO	0.11	0.05	0.13	b.d.	0.05	0.09	0.55	0.03	0.09	0.06
CaO	0.04	b.d.	0.03	0.06	0.03	0.03	0.15	0.02	0.03	0.05
F	b.d.	b.d.	b.d.	b.d.	b.d.	b.d.	b.d.	b.d.	b.d.	b.d.
Cl	0.12	b.d.	b.d.	0.04	b.d.	0.05	0.08	0.04	b.d.	0.11
-O=F,Cl	b.d.	b.d.	b.d.	b.d.	b.d.	b.d. b.d. b.d.	b.d.	b.d.	b.d.	b.d.
total	98.34	97.48	99.98	99.23	97.51	100.14	98.54	98.11	99.83	100.07

Element	Porous domains					Overgrowth/rims				
wt%	LL169-2-36	LL169-2-38	LL169-2-40	LL169-2-41	LL169-2-47	LL169-1-3	LL169-1-41	LL169-1-42	LL169-1-45	LL169-1-47
SiO_2	33.84	33.52	33.87	32.91	33.12	33.22	33.82	33.22	33.59	31.69
ZrO_2	62.99	64.73	64.40	62.72	63.02	61.77	62.26	58.93	62.64	57.92
HfO_2	1.46	1.49	1.60	1.47	1.41	1.24	1.37	1.40	1.48	1.19
ThO_2	0.62	0.03	0.00	0.54	0.14	0.70	1.10	0.88	0.44	0.61
Y_2O_3	0.04	0.14	b.d.	b.d.	0.56	1.70	1.34	2.54	0.52	3.32
P_2O_5	b.d.	b.d.	b.d.	b.d.	b.d.	b.d.	b.d.	b.d.	b.d.	0.20
FeO	0.16	0.06	0.07	0.26	0.08	0.06	0.05	b.d.	0.06	0.15
CaO	0.03	0.03	b.d.	0.06	0.04	b.d.	0.05	b.d.	0.03	0.04
F	b.d.	b.d.	b.d.	b.d.	b.d.	b.d.	b.d.	b.d.	b.d.	b.d.
Cl	b.d.	b.d.	b.d.	0.05	0.14	b.d.	b.d.	b.d.	b.d.	b.d.
-O=F,Cl	b.d.	b.d.	b.d.	b.d.	b.d.	b.d.	b.d.	b.d.	b.d.	b.d.
total	99.14	100.00	99.95	98.00	98.50	98.71	100.00	97.01	98.76	95.13

Element	Overgrowth/rims								
wt%	LL169-2-2	LL169-2-8	LL169-2-18	LL169-2-28	LL169-2-30	LL169-2-37	LL169-2-44	LL169-2-45	LL169-2-46
SiO_2	33.80	33.22	32.64	33.42	33.33	34.11	33.39	32.76	33.23
ZrO_2	64.37	61.16	60.03	60.15	64.58	63.32	62.85	59.07	59.93
HfO_2	1.43	1.27	1.30	1.30	1.38	1.61	1.27	1.52	1.35
ThO_2	0.18	0.88	1.00	0.83	0.80	0.44	0.71	0.61	0.50
Y_2O_3	b.d.	1.49	1.92	2.29	b.d.	0.65	0.76	3.15	2.41
P_2O_5	b.d.	b.d.	b.d.	b.d.	b.d.	b.d.	b.d.	b.d.	b.d.
FeO	b.d.	b.d.	b.d.	0.09	b.d.	b.d.	b.d.	b.d.	0.05
CaO	b.d.	0.04	0.05	b.d.	0.03	b.d.	0.03	b.d.	b.d.
F	b.d.	b.d.	b.d.	b.d.	b.d.	b.d.	b.d.	b.d.	b.d.
Cl	b.d.	b.d.	b.d.	b.d.	b.d.	b.d.	b.d.	b.d.	b.d.
-O=F,Cl	b.d.	b.d.	b.d.	b.d.	b.d.	b.d.	b.d.	b.d.	b.d.
total	99.85	98.08	96.96	98.10	100.13	100.14	99.04	97.13	97.50

Table A2

Trace elemental concentrations of zircon from altered tuff and gabbros

Magmatic zircon from altered tuff	LL12-1	LL12-2	LL12-3	LL12-4	LL12-5	LL12-6	LL12-7	LL12-8	LL12-9	LL12-10	LL12-11	LL12-12	LL12-13	LL12-14	LL12-15
wt.% (convert from trace elements)															
HfO_2	0.93	1.01	1.04	1.05	1.04	1.03	1.03	0.98	0.99	1.03	0.98	1.00	0.99	1.00	1.26
ThO_2	0.02	0.01	0.01	0.01	0.01	0.01	0.01	0.03	0.01	0.01	0.01	0.01	0.01	0.01	0.02
Y_2O_3	0.18	0.13	0.15	0.16	0.27	0.15	0.21	0.47	0.36	0.15	0.28	0.23	0.27	0.13	0.30
P_2O_5	0.09	0.08	0.08	0.08	0.06	0.08	0.07	0.10	0.07	0.08	0.07	0.07	0.06	0.07	0.08
FeO	0.01	0.02	0.01	0.01	0.01	0.00	0.16	0.02	0.01	0.00	0.02	0.02	0.01	0.00	0.04
CaO	0.00	0.00	0.00	0.00	0.00	0.00	0.00	0.01	0.00	0.01	0.00	0.03	0.00	0.02	0.03
ppm															
Mg	1.37	1.25	0.58	1.71	0.00	0.90	0.47	1.46	1.29	0.00	1.25	0.07	0.00	0.00	1.92
Al	0.00	2.13	0.00	2.32	0.62	0.00	492	0.50	0.97	0.00	0.00	0.00	0.00	1.15	4.14
P	396	331	356	347	281	364	304	454	320	346	310	286	280	297	338
Ca	0.00	0.00	0.00	0.00	20.24	0.00	30.92	78.36	0.00	44.22	0.00	200.15	0.00	123.73	231
Sc	116	111	105	104	103	108	104	108	103	110	103	101	104	104	87
Ti	15.2	12.8	12.3	8.70	11.0	8.9	25.6	15.5	11.4	11.5	8.60	10.7	10.7	13.0	3.6
V	0.07	0.03	0.00	0.00	0.00	0.00	0.00	0.00	0.00	0.03	0.01	0.00	0.08	0.00	0.16
Cr	0.97	0.00	0.75	0.00	0.00	2.16	0.00	0.19	0.00	2.44	0.00	1.69	1.70	2.44	3.11
Mn	0.06	0.00	0.10	0.13	0.00	0.00	0.13	0.22	0.00	0.13	0.17	0.31	0.00	0.00	1.54
Fe	47.5	122	50.4	83.8	61.9	20.2	1237	161	81.0	7.03	133	133	49.8	0.00	286
Rb	0.17	0.07	0.02	0.26	0.22	0.16	1.11	0.57	0.33	0.21	0.24	0.21	0.15	0.13	0.35
Sr	0.14	0.09	0.14	0.20	0.20	0.16	0.29	0.31	0.24	0.14	0.22	0.16	0.11	0.15	0.67
Y	1435	1028	1165	1266	2124	1144	1642	3723	2872	1214	2182	1829	2105	1003	2324
Nb	13.2	9.8	14.0	16.6	6.8	12.6	13.5	23.5	11.0	14.0	16.0	13.8	6.7	10.5	52.2
Ba	0.03	0.02	0.02	0.10	0.04	0.03	7.32	0.03	0.10	0.05	0.03	0.03	0.08	0.07	2.51
La	0.03	0.01	0.01	0.01	0.03	0.01	1.37	0.08	0.05	0.00	0.05	0.02	0.06	0.00	0.25
Ce	13.2	7.01	10.0	11.0	7.01	9.17	10.8	15.1	9.01	9.50	8.09	8.44	6.86	7.60	21.3
Pr	0.23	0.11	0.07	0.13	0.41	0.11	0.55	0.56	0.54	0.17	0.37	0.30	0.32	0.11	0.33
Nd	3.56	2.26	2.49	2.81	7.05	2.44	5.81	9.71	7.95	2.51	4.86	4.14	6.32	2.05	3.76
Sm	8.01	4.68	6.08	6.15	13.04	6.03	9.70	24.54	17.29	5.46	10.77	10.10	13.11	4.87	9.96
Eu	1.53	1.24	1.29	1.28	3.08	1.28	2.10	4.98	4.17	1.34	2.55	2.17	2.90	1.15	1.78
Gd	39.8	26.5	30.5	32.1	65.0	29.2	50.0	121.1	92.5	29.6	60.2	53.0	60.9	25.1	54.4
Tb	13.5	8.40	10.2	10.5	20.5	9.48	15.6	36.6	28.3	9.83	19.3	16.3	19.7	8.17	18.9
Dy	157	107	124	134	240	119	179	427	325	126	235	203	228	103	238
Ho	54.5	38.0	44.3	47.4	80.8	41.5	61.7	141	109	43.9	80.8	69.2	78.8	36.5	85.4
Er	237	169	197	212	349	191	265	600	465	198	356	298	339	166	378
Tm	45.7	34.7	40.1	42.1	66.4	38.2	52.6	113	88.0	39.6	69.1	58.0	64.6	33.2	73.8
Yb	385	300	345	364	554	327	437	916	731	349	581	485	537	292	599
Lu	64.7	52.5	60.5	62.9	94.3	57.1	77.4	157	124	61.1	102	87.1	93.1	51.2	100
Hf	7898	8526	8801	8878	8794	8775	8692	8325	8435	8698	8323	8464	8388	8468	10679
Ta	4.57	3.87	5.22	5.84	3.18	5.00	4.37	7.20	4.24	5.10	5.48	5.23	3.24	4.56	14.49
Pb	32.9	11.4	16.6	16.6	13.9	15.9	15.0	51.8	20.6	19.7	15.0	14.6	12.2	13.7	30.7
Th	174	62.9	95.9	95.5	77.0	91.1	82.4	289	116	113	87.9	81.3	72.4	78.2	205
U	180	95.8	137	136	114	131	120	263	159	151	155	126	106	115	300

Magmatic zircon from altered tuff	LL12-16	LL12-17	LL12-18	LL12-19	LL12-20	LL12-21	LL12-22	LL12-23	LL12-24	LL12-25	LL12-26	LL12-27	LL12-28	LL12-29	LL12-30
wt.% (convert from trace elements)															
HfO_2	0.96	0.97	0.98	0.94	0.99	0.97	0.94	0.93	0.87	0.93	0.95	0.96	0.95	0.98	0.93
ThO_2	0.01	0.01	0.01	0.01	0.01	0.01	0.01	0.02	0.00	0.00	0.01	0.01	0.01	0.01	0.01
Y_2O_3	0.13	0.12	0.16	0.15	0.25	0.30	0.30	0.21	0.16	0.18	0.20	0.26	0.27	0.12	0.24
P_2O_5	0.08	0.07	0.07	0.07	0.05	0.06	0.05	0.08	0.05	0.05	0.07	0.05	0.05	0.05	0.06
FeO	0.01	0.01	0.02	0.01	0.01	0.01	0.01	0.01	0.01	0.01	0.01	0.02	0.01	0.00	0.01
CaO	0.00	0.00	0.00	0.02	0.02	0.00	0.00	0.00	0.02	0.03	0.01	0.00	0.00	0.00	0.00
ppm															
Mg	0.00	0.00	1.94	0.25	0.68	0.70	0.70	0.00	0.07	1.31	0.27	0.39	0.84	0.00	0.25
Al	0.00	0.00	2.14	0.00	0.00	2.37	1.95	5.11	0.36	1.32	0.35	0.12	0.00	0.00	0.00
P	331	301	291	298	232	243	235	353	200	200	287	218	224	225	271
Ca	0.00	0.00	0.00	131	119	0.00	0.00	6.15	163	185	36.1	0.00	0.00	3.88	8.18
Sc	107	110	105	100	98	94	105	102	109	108	103	99.1	102	98.6	105
Ti	11.2	17.2	11.3	9.70	8.26	10.3	10.1	16.3	11.6	11.7	11.8	8.09	12.1	9.88	9.76
V	0.05	0.10	0.13	0.02	0.07	0.01	0.04	0.13	0.00	0.06	0.00	0.01	0.14	0.00	0.09
Cr	0.36	0.00	0.98	0.00	0.00	0.73	0.93	0.00	0.00	0.00	0.55	2.09	0.11	0.16	1.14
Mn	0.00	0.24	0.25	0.15	0.00	0.00	0.00	0.38	0.02	0.00	0.31	0.17	0.53	0.08	0.23
Fe	106	67.3	141	101	103	70.3	97.2	46.0	68.7	100	105	119	98.5	21.6	106
Rb	0.28	0.17	0.27	0.08	0.25	0.23	0.35	0.19	0.29	0.42	0.26	0.40	0.29	0.17	0.29
Sr	0.15	0.15	0.25	0.09	0.18	0.18	0.24	0.19	0.12	2.02	0.10	0.22	0.24	0.19	0.21
Y	1034	912	1242	1188	1952	2373	2352	1644	1259	1453	1571	2064	2127	980	1876
Nb	9.71	7.67	15.9	13.2	6.62	8.83	7.51	27.4	3.31	3.71	13.8	7.04	6.48	10.3	7.58
Ba	0.05	0.00	0.08	0.08	0.02	0.10	0.04	0.12	0.00	0.03	0.02	0.08	0.02	0.06	0.21
La	0.00	0.01	0.00	0.01	0.00	0.04	0.05	0.75	0.00	0.00	0.02	0.02	0.03	0.01	0.04
Ce	6.46	6.06	8.35	9.24	6.92	8.55	6.25	16.3	5.56	4.59	8.76	6.78	6.26	7.73	5.62
Pr	0.09	0.09	0.11	0.14	0.37	0.42	0.44	0.45	0.26	0.29	0.23	0.30	0.41	0.06	0.36
Nd	1.93	1.89	3.11	2.80	5.93	7.00	7.16	4.82	4.46	5.09	3.23	6.05	6.60	1.86	5.97
Sm	4.15	4.09	5.90	5.66	11.3	14.8	13.8	8.87	8.86	9.62	7.76	12.1	11.84	4.39	10.9
Eu	1.00	0.99	1.34	1.28	2.33	3.20	2.97	1.64	1.83	2.26	1.76	2.88	2.94	0.98	2.54
Gd	25.9	21.2	30.5	29.2	59.1	74.1	70.7	42.2	38.8	43.3	41.0	59.1	61.8	22.4	53.5
Tb	8.49	7.18	9.92	9.71	18.1	22.2	21.4	13.9	11.8	13.1	13.1	18.7	19.4	7.78	17.1
Dy	105	89.8	121	118	214	262	258	166	137	155	159	220	232	98.8	200
Ho	37.0	32.1	44.5	41.7	72.3	87.4	86.0	58.7	44.9	51.9	55.9	75.6	77.3	34.9	68.9
Er	167	145	199	190	304	367	367	260	196	225	245	322	331	157	294
Tm	34.7	29.2	39.1	37.6	57.6	69.8	69.1	49.4	36.5	43.3	48.0	59.9	63.4	31.8	56.5
Yb	298	262	333	327	470	572	567	421	309	373	406	497	521	269	457
Lu	53.9	46.2	60.6	59.1	83.6	99.3	101	73.6	55.7	64.0	73.5	87.5	89.1	48.7	82.7
Hf	8170	8258	8304	8010	8415	8265	7955	7921	7404	7848	8087	8118	8033	8341	7910
Ta	4.18	3.23	6.48	4.88	2.96	3.36	3.34	8.05	1.62	2.16	5.29	3.07	2.70	3.93	3.45
Pb	11.0	9.82	11.2	20.4	11.5	16.9	14.7	31.9	7.99	7.2	17.3	12.9	12.2	10.3	10.8
Th	62.3	57.1	61.7	116	67.9	93.2	84.1	188	41.3	40.8	101	72.1	74.1	60.8	64.8
U	102	90.9	97.6	151	96.8	130	114	191	61.8	62.0	137	101	103	97.7	91.6

Table A2

(continued)

Zircon from altered gabbros												
	Unmodified zircon		Inclusion-free domains									
	LL169-1-6	LL169-2-7	LL169-1-1	LL169-1-2	LL169-1-3	LL169-1-5	LL169-1-14	LL169-1-18	LL169-1-21	LL169-1-26	LL169-2-1	LL169-2-5
ppm												
Mg	394	34.9	50.3	1099	1170	451	2285	2036	2849	354	852	2223
Al	21.8	16.4	42	551	638	338	1043	1249	1404	132	382	1083
P	409	826	1830	1493	791	900	2450	1928	2355	2306	2214	1571
Ca	137	38.9	473	3997	529	633	443	1565	359	294	701	656
Sc	106	92.8	182	162	156	116	140	164	137	170	137	191
Ti	32.6	39.3	21.9	53.8	35.9	69.7	33.2	97.4	83.0	16.9	35.5	65.6
V	0.75	0.26	1.30	6.35	3.04	6.03	10.75	12.12	10.49	3.13	4.11	6.94
Mn	10.5	4.65	152.9	176.0	64.7	65.7	118.2	146.0	108.3	117.8	72.0	97.3
Fe	1505	703	2057	5950	3733	7758	7688	20841	15429	4020	11190	11041
Rb	1.38	0.76	5.51	5.67	2.31	1.14	5.68	2.92	2.32	3.12	2.57	2.94
Sr	1.94	0.86	17.2	16.0	10.2	8.93	14.3	20.5	13.3	19.0	10.7	19.1
Y	1591	2841	20271	11613	5975	3897	17374	12330	12327	21308	10739	10675
Nb	8.10	11.6	25.8	28.6	19.6	34.3	36.8	35.6	51.8	31.1	32.9	25.9
Ba	5.80	2.22	40.6	22.4	39.4	7.86	44.9	52.8	23.1	35.7	34.4	153
La	0.23	0.24	6.86	7.55	17.51	2.59	5.08	12.60	4.43	2.79	2.33	5.68
Ce	41.9	74.7	621	333	213	124	412	289	347	587	211	281
Pr	0.26	0.38	30.59	11.22	10.48	2.40	11.82	11.67	11.22	15.66	8.35	12.84
Nd	3.40	5.92	375	125	80.2	25.0	156	126	142	211	107	146
Sm	7.79	15.2	470	161	72.30	29.04	218	162	186	305	149	177
Eu	0.75	1.50	29.18	12.26	9.05	5.02	14.34	11.99	16.61	21.63	10.88	17.12
Gd	39.2	80.6	1323	533	227	111	718	520	639	1041	490	546
Tb	13.3	26.7	336	145	67	34	197	143	173	287	130	143
Dy	158	305	2952	1432	675	380	1910	1351	1652	2727	1232	1330
Ho	52	98	728	409	211	128	557	391	460	739	349	376
Er	230	399	2412	1569	896	566	2200	1580	1694	2639	1351	1481
Tm	45.6	74.4	377	269	167	109	396	292	277	448	243	272
Yb	381	601	2531	2012	1374	908	3038	2392	2048	3218	1944	2309
Lu	68.7	93.4	330	300	256	156	474	434	301	453	310	466
Hf	9087	9784	9504	9690	9418	9844	9137	10289	9113	9693	10363	11334
Ta	4.58	5.94	11.23	9.14	5.98	14.40	10.96	8.51	26.43	6.10	10.55	4.80
Pb	53.4	176	363	284	1236	177	445	1114	86.6	377	1057	522
Th	303	955	2071	2332	1655	2164	3575	4186	1385	2508	1945	3065
U	234	298	1285	924	679	904	960	1192	1297	988	913	963

Zircon from altered gabbros												
	Inclusion-free domains											
	LL169-2-8	LL169-2-10	LL169-2-12	LL169-2-15	LL169-1-4	LL169-1-9	LL169-1-12	LL169-2-4	LL169-2-9	LL169-2-14	LL169-2-20	LL169-2-21
ppm												
Mg	387	572	650	1426	2693	2090	1421	3436	1514	522	984	3073
Al	224	503	442	796	1218	1129	770	1859	696	599	416	1560
P	2021	1622	3149	1870	2326	1562	1749	901	2405	3157	2403	1770
Ca	723	522	802	938	753	1157	1122	3042	619	1366	1002	2321
Sc	144	152	131	108	129	168	130	146	134	147	145	140
Ti	25.0	18.1	112	97.5	152.3	69.7	56.4	96.3	59.2	135.7	67.9	53.0
V	3.07	2.31	6.47	8.19	13.6	8.01	7.69	11.9	7.28	7.54	5.97	13.3
Mn	93.1	52.6	148	112	185	139	110	163	77.6	204	171	94.8
Fe	8251	2789	10804	11478	21086	12394	8525	27841	10590	10204	9144	12276
Rb	4.78	3.74	1.80	2.78	2.60	2.27	2.59	5.06	2.58	2.63	1.92	2.12
Sr	16.9	7.04	22.3	14.7	13.6	23.5	14.7	17.0	16.0	36.1	22.9	13.4
Y	8426	10627	13221	7364	13897	10437	8087	4884	10533	14665	14064	7100
Nb	60.4	31.3	76.0	39.8	62.0	41.9	40.1	22.3	35.2	89.7	63.9	38.7
Ba	34.5	16.7	24.5	17.2	31.3	37.3	20.2	43.3	30.7	46.0	28.9	16.5
La	2.99	2.31	3.30	11.16	2.97	3.61	4.97	19.85	1.73	9.16	4.52	11.49
Ce	176	268	525	216	324	300	198	180	206	568	527	239
Pr	5.95	4.79	9.53	7.10	9.01	7.85	7.32	8.29	6.64	18.45	9.82	9.72
Nd	71.0	68.7	132	67.9	114	102	86.5	63.2	89.8	207	122	94.3
Sm	96.2	110	188	74.1	144	146	104	49.9	132	242	177	104
Eu	7.40	9.04	17.6	9.78	11.2	12.7	12.1	8.04	9.92	33.4	15.8	12.0
Gd	327	431	681	294	491	494	345	167	463	789	660	349
Tb	91.7	125	181	82.9	140	133	96.1	48.0	126	204	180	89.2
Dy	928	1273	1744	830	1486	1255	925	509	1246	1893	1765	851
Ho	283	372	481	247	462	356	280	165	363	519	488	248
Er	1167	1458	1717	971	1927	1411	1088	732	1408	1922	1771	981
Tm	227	263	285	175	354	259	197	142	255	331	308	187
Yb	1943	2031	2164	1370	2790	2205	1560	1271	1987	2546	2249	1568
Lu	327	342	329	220	476	440	254	267	317	431	326	266
Hf	9599	10005	10179	10057	8520	11251	9658	9594	10441	9463	9591	9569
Ta	14.7	10.8	23.2	13.6	15.3	15.0	11.9	9.23	13.3	25.4	21.6	7.96
Pb	137	193	146	200	272	269	178	153	190	187	352	132
Th	1647	1369	2746	2402	3042	3763	3373	1542	1722	3295	5086	2877
U	1223	1043	1410	1027	1434	1294	1125	1008	983	1823	1666	1085

Table A2
(continued)

Zircon from altered gabbros												
	Porous domains											
	LL169-1-20	LL169-2-3	LL169-2-18	LL169-1-7	LL169-1-8	LL169-1-11	LL169-1-13	LL169-1-15	LL169-1-16	LL169-1-17	LL169-1-19	LL169-1-22
ppm												
Mg	2192	804	3066	371	5198	1784	2134	1176	747	1845	691	557
Al	1078	451	1577	256	3094	1125	1316	712	406	1295	433	343
P	1518	715	609	621	294	276	365	1135	431	343	315	501
Ca	1916	2424	2572	864	959	414	851	7747	233	2338	442	627
Sc	136	155	115	131	114	110	103	219	109	238	93.5	99.4
Ti	348	35.2	51.1	54.8	30.5	78.8	48.3	60.7	27.5	122	2227	46.4
V	13.4	3.13	7.27	1.65	11.8	3.84	6.34	4.28	1.71	5.60	4.93	2.34
Mn	124	87.1	52.1	54.3	71.1	37.0	48.1	179	32.7	128	233	62.5
Fe	30283	5847	7115	4757	16278	5716	8673	14143	3015	13303	8302	6332
Rb	4.27	1.82	1.75	1.70	1.22	3.18	1.86	1.96	1.40	3.95	0.99	6.83
Sr	24.7	13.4	7.16	10.1	7.45	10.6	5.17	32.3	6.30	18.4	6.66	9.05
Y	7032	2811	2332	2346	1463	1152	1382	5849	1888	3481	1020	1790
Nb	27.0	25.7	26.4	29.7	14.9	6.77	13.3	39.2	9.17	18.8	15.2	8.47
Ba	75.1	9.44	11.3	12.1	12.1	54.0	11.8	56.9	20.3	35.7	11.3	22.3
La	3.04	7.14	1.32	1.26	1.78	1.17	1.58	5.47	0.58	11.82	3.98	1.01
Ce	126	58.4	60.3	43.6	25.8	18.3	30.9	60.4	43.9	108	19.7	35.7
Pr	3.52	3.18	1.01	0.98	0.99	0.51	0.69	4.15	0.41	11.59	1.24	0.53
Nd	38.6	21.1	9.92	9.32	8.71	3.35	5.84	33.2	5.40	80.1	7.11	6.36
Sm	47.9	9.83	14.4	11.3	7.55	3.80	6.88	27.8	7.87	30.8	3.99	9.04
Eu	4.02	2.00	2.25	1.65	1.50	0.75	0.97	6.57	1.25	14.6	0.62	0.96
Gd	184	28.3	61.4	49.3	26.3	17.6	28.3	90.8	38.5	65.4	15.5	42.1
Tb	58.9	9	18.8	15.1	9	6	9	27.9	13.4	17.9	6	14.4
Dy	654	140	215	180	107	81.8	115	361	165	220	73.7	166
Ho	232	75.5	72.5	70.8	43.9	34.8	43.2	159	61.9	97.2	31.0	58.7
Er	1063	497	335	371	240	191	219	918	295	574	172	274
Tm	210	127	73.4	83.3	55.8	44.5	48.1	213	60.4	136	40.6	55.2
Yb	1817	1370	704	827	589	459	461	2177	540	1529	404	492
Lu	352	326	158	194	153	118	98.8	523	107	458	84.1	92.1
Hf	8052	9938	10087	8791	10802	11310	9353	10226	10371	7976	10975	10558
Ta	8.55	4.49	8.54	9.22	6.27	3.15	6.08	9.92	4.32	4.27	5.93	4.39
Pb	216	80.9	95.7	95.9	66.5	82.9	90.6	1114	132	112	56.9	75.7
Th	1674	1402	967	760	489	540	600	2486	803	1378	503	479
U	1055	1220	717	852	566	386	408	1396	372	1070	411	348

Zircon from altered gabbros											
	Porous domains							Overgrowth/rims			
	LL169-1-24	LL169-1-25	LL169-2-6	LL169-2-11	LL169-2-13	LL169-2-16	LL169-2-17	LL169-1-31	LL169-1-32	LL169-1-33	LL169-1-10
ppm											
Mg	854	1565	1485	2209	1712	2903	716	N.A.	N.A.	N.A.	36.1
Al	574	878	824	1140	667	1321	492	N.A.	N.A.	N.A.	24.7
P	204	245	426	325	246	216	269	1192	355	1105	500
Ca	973	2538	8897	3099	7594	1558	3701	N.A.	N.A.	N.A.	164
Sc	179	190	231	163	135	117	246	N.A.	N.A.	N.A.	119
Ti	35.8	34.1	56.5	127	81.0	22.5	65.7	136	75.0	150	34.8
V	3.23	4.74	3.27	9.63	7.15	5.58	4.31	N.A.	N.A.	N.A.	6.24
Mn	51.7	56.1	133	100	98.5	47.5	112.3	N.A.	N.A.	N.A.	99.2
Fe	5158	6608	11728	9599	13032	8275	12734	N.A.	N.A.	N.A.	144
Rb	1.38	2.25	3.17	2.01	1.28	0.93	2.56	N.A.	N.A.	N.A.	1.63
Sr	10.2	13.1	35.1	14.4	20.1	7.54	26.0	N.A.	N.A.	N.A.	15.7
Y	2423	2710	3050	1767	1438	1064	3533	N.A.	N.A.	N.A.	2220
Nb	14.2	13.7	12.7	29.1	14.9	13.8	14.5	36.0	16.2	32.1	34.8
Ba	29.2	35.4	47.5	22.1	31.2	14.5	37.5	N.A.	N.A.	N.A.	13.7
La	0.57	0.70	2.75	0.67	0.94	1.10	2.03	70.88	169	117	83.0
Ce	10.9	22.5	25.0	11.1	12.3	14.2	21.7	271	486	357	280
Pr	0.61	0.62	1.84	0.65	0.76	0.81	1.64	22.24	62.28	37.96	23.52
Nd	5.56	6.75	14.4	4.49	5.67	7.33	12.9	119	277	189	116
Sm	5.24	7.51	10.5	3.32	3.23	3.58	8.43	64.4	59.5	63.6	29.7
Eu	1.24	1.41	5.52	1.26	1.43	1.53	3.74	6.33	7.79	9.37	3.95
Gd	20.8	33.0	35.8	13.8	12.9	13.9	35.2	222	70.6	162	56.5
Tb	7.21	11.4	11.5	4.62	4.56	4.58	10.6	69.2	16.4	46.5	15.4
Dy	104	151	162	79.7	69.4	64.5	166	740	170	502	177
Ho	63.2	73.8	83.4	45.5	38.2	29.7	91.0	242	64.1	174	66.9
Er	450	470	534	316	256	181	616	1040	333	810	339
Tm	117	115	133	85.0	66.1	45.4	159	198	76.8	171	73.1
Yb	1424	1361	1515	1028	768	522	1914	1663	814	1624	707
Lu	495	435	458	316	231	147	645	307	211	352	158
Hf	10028	10274	10417	10187	9899	11790	9448	15108	13607	16162	10191
Ta	2.23	3.24	2.57	8.07	4.09	6.16	1.79	11.9	6.18	9.94	13.6
Pb	69.1	90.2	140	84.8	77.5	59.1	102	11.4	5.88	11.9	92.7
Th	624	713	1566	741	640	488	1103	2472	868	1651	913
U	848	713	1135	717	604	489	1223	1062	637	1221	809

TABLE A3

U-Th-Pb isotopic compositions of different zircon in the altered gabbros

	Th/U	$^{207}Pb/^{206}Pb$ Ratio	1σ	$^{207}Pb/^{235}U$ Ratio	1σ	$^{206}Pb/^{238}U$ Ratio	1σ	$^{208}Pb/^{232}Th$ Ratio	1σ	$^{207}Pb/^{206}Pb$ Age (Ma)	1σ	$^{207}Pb/^{235}U$ Age (Ma)	1σ	$^{206}Pb/^{238}U$ Age (Ma)	1σ	$^{208}Pb/^{232}Th$ Age (Ma)	1σ	Con.
Unmodified, magmatic zircon																		
LL169-17	1.19	0.1050	0.0002	4.4128	0.0193	0.3047	0.0012	0.0951	0.0007	1717	2	1715	4	1714	6	1836	14	99%
LL169-63	2.34	0.1055	0.0002	4.4673	0.0208	0.3071	0.0014	0.0914	0.0007	1724	4	1725	4	1727	7	1768	12	99%
LL169-66	2.06	0.1046	0.0002	4.4245	0.0209	0.3067	0.0012	0.0966	0.0007	1706	4	1717	4	1725	6	1864	13	99%
LL169-89	1.14	0.1065	0.0004	3.9856	0.0378	0.2710	0.0021	0.0768	0.0014	1740	7	1631	8	1546	10	1495	27	94%
Inclusion-free domains																		
LL169-04	1.42	0.1057	0.0005	3.4427	0.0754	0.2340	0.0043	0.0821	0.0013	1726	42	1514	17	1355	22	1594	25	88%
LL169-08	1.73	0.1050	0.0003	3.6370	0.0283	0.2509	0.0017	0.0781	0.0010	1715	5	1558	6	1443	9	1520	18	92%
LL169-15	1.28	0.1064	0.0007	4.4335	0.0612	0.3012	0.0027	0.0760	0.0032	1739	11	1719	11	1697	14	1480	60	98%
LL169-22	1.84	0.1042	0.0003	4.3127	0.0592	0.2999	0.0034	0.0958	0.0024	1700	6	1696	11	1691	17	1849	43	99%
LL169-23	1.42	0.1056	0.0004	4.4541	0.0499	0.3059	0.0036	0.0862	0.0009	1725	7	1722	9	1721	18	1671	17	99%
LL169-31	2.51	0.1057	0.0002	3.7064	0.0228	0.2543	0.0014	0.0760	0.0007	1726	5	1573	5	1461	7	1481	13	92%
LL169-34	1.17	0.1043	0.0004	3.8143	0.0156	0.2651	0.0010	0.0895	0.0006	1703	7	1596	3	1516	5	1733	12	94%
LL169-37	2.36	0.1054	0.0003	4.4619	0.0746	0.3055	0.0043	0.0922	0.0017	1721	6	1724	14	1718	21	1782	31	99%
LL169-38	1.54	0.1066	0.0005	4.3147	0.0480	0.2932	0.0021	0.1005	0.0012	1743	9	1696	9	1657	11	1935	21	97%
LL169-40	1.29	0.1052	0.0003	4.0480	0.0219	0.2792	0.0017	0.0876	0.0009	1718	5	1644	4	1587	8	1697	17	96%
LL169-44	2.37	0.1016	0.0003	2.7059	0.0270	0.1929	0.0014	0.0542	0.0005	1654	7	1330	7	1137	8	1068	10	84%
LL169-50	1.03	0.1050	0.0004	3.6185	0.0296	0.2498	0.0018	0.0752	0.0008	1717	8	1554	7	1438	9	1466	15	92%
LL169-56	0.80	0.1048	0.0002	4.1284	0.0211	0.2857	0.0015	0.0856	0.0007	1710	4	1660	4	1620	7	1660	13	97%
LL169-45	1.63	0.1051	0.0004	3.4504	0.0321	0.2380	0.0017	0.0719	0.0007	1717	6	1516	7	1376	9	1404	13	90%
LL169-47	1.05	0.1053	0.0008	3.5046	0.0444	0.2410	0.0016	0.0795	0.0006	1720	47	1528	10	1392	8	1546	11	90%
LL169-72	3.44	0.1047	0.0005	3.4548	0.0507	0.2386	0.0024	0.0664	0.0010	1709	9	1517	12	1379	12	1300	19	90%
LL169-74	2.24	0.1053	0.0003	3.7009	0.0256	0.2549	0.0019	0.0743	0.0007	1720	5	1572	6	1464	10	1449	13	92%
LL169-76	2.32	0.1068	0.0003	4.4645	0.0442	0.3038	0.0026	0.0934	0.0011	1746	5	1724	8	1710	13	1805	20	99%
LL169-78	1.47	0.1051	0.0002	3.5135	0.0141	0.2424	0.0011	0.0730	0.0005	1717	2	1530	3	1399	6	1423	9	91%
LL169-80	1.37	0.1049	0.0003	3.6769	0.0269	0.2544	0.0021	0.0809	0.0008	1722	5	1566	6	1461	11	1573	14	93%
LL169-82	0.93	0.1042	0.0002	3.6036	0.0341	0.2507	0.0023	0.0746	0.0009	1700	2	1550	8	1442	12	1455	18	92%
LL169-84	0.84	0.1059	0.0002	4.1965	0.0249	0.2871	0.0015	0.0829	0.0005	1731	36	1673	5	1627	8	1611	10	97%
LL169-88	1.06	0.1024	0.0005	3.2432	0.0674	0.2286	0.0039	0.0778	0.0113	1678	11	1468	16	1327	20	1515	212	89%
LL169-93	1.14	0.1063	0.0003	4.0211	0.0259	0.2743	0.0015	0.0879	0.0006	1736	5	1638	5	1563	8	1703	11	95%
LL169-101	2.17	0.1040	0.0002	3.8248	0.0257	0.2666	0.0018	0.0798	0.0008	1698	4	1598	5	1523	9	1553	15	95%
LL169-99	1.44	0.1051	0.0002	4.0794	0.0169	0.2814	0.0011	0.0826	0.0006	1717	2	1650	3	1599	6	1604	11	96%

TABLE A3

(continued)

	Th/U	$^{207}Pb/^{206}Pb$ Ratio	1σ	$^{207}Pb/^{235}U$ Ratio	1σ	$^{206}Pb/^{238}U$ Ratio	1σ	$^{208}Pb/^{232}Th$ Ratio	1σ	$^{207}Pb/^{206}Pb$ Age (Ma)	1σ	$^{207}Pb/^{235}U$ Age (Ma)	1σ	$^{206}Pb/^{238}U$ Age (Ma)	1σ	$^{208}Pb/^{232}Th$ Age (Ma)	1σ	Con.
Unmodified, magmatic zircon																		
Porous domains																		
LL169-03	1.41	0.1154	0.0005	4.0648	0.0160	0.2558	0.0012	0.0888	0.0007	1887	7	1647	3	1468	6	1720	12	88%
LL169-05	1.04	0.0917	0.0002	2.1703	0.0103	0.1718	0.0010	0.0610	0.0009	1461	5	1172	3	1022	6	1196	16	86%
LL169-11	1.03	0.0943	0.0003	2.5351	0.0216	0.1946	0.0012	0.0811	0.0010	1515	6	1282	6	1146	6	1576	18	88%
LL169-12	1.30	0.1011	0.0003	2.8239	0.0173	0.2026	0.0011	0.0733	0.0010	1644	6	1362	5	1189	6	1431	19	86%
LL169-13	1.62	0.0820	0.0002	1.7796	0.0075	0.1575	0.0006	0.0442	0.0004	1256	5	1038	3	943	3	873	8	90%
LL169-14	0.79	0.0816	0.0002	1.8374	0.0085	0.1634	0.0007	0.0572	0.0004	1235	4	1059	3	975	4	1125	7	91%
LL169-16	1.17	0.0896	0.0002	2.5485	0.0186	0.2060	0.0012	0.0714	0.0006	1418	4	1286	5	1208	6	1394	12	93%
LL169-18	1.81	0.0837	0.0002	1.3853	0.0105	0.1201	0.0008	0.0277	0.0003	1285	10	883	4	731	5	553	6	81%
LL169-26	1.27	0.0883	0.0003	2.1970	0.0124	0.1802	0.0006	0.0587	0.0004	1391	6	1180	4	1068	3	1152	8	90%
LL169-27	1.42	0.0965	0.0003	3.0048	0.0198	0.2257	0.0013	0.0868	0.0010	1558	6	1409	5	1312	7	1682	19	92%
LL169-29	2.16	0.1304	0.0006	4.4754	0.0475	0.2485	0.0018	0.0841	0.0009	2103	14	1726	9	1431	9	1632	17	81%
LL169-30	1.34	0.0961	0.0005	3.2479	0.0273	0.2446	0.0012	0.0910	0.0008	1550	8	1469	7	1410	6	1760	14	95%
LL169-32	0.69	0.0920	0.0005	2.3949	0.0150	0.1887	0.0007	0.0790	0.0007	1533	11	1241	4	1115	4	1536	13	89%
LL169-35	1.68	0.1014	0.0002	3.4515	0.0256	0.2467	0.0018	0.0877	0.0010	1651	4	1516	6	1421	9	1699	18	93%
LL169-36	1.35	0.1114	0.0004	3.8880	0.0287	0.2532	0.0017	0.0979	0.0015	1822	6	1611	6	1455	9	1888	28	89%
LL169-39	1.48	0.0971	0.0002	3.2907	0.0174	0.2458	0.0012	0.0781	0.0009	1569	4	1479	4	1417	6	1519	17	95%
LL169-41	1.16	0.0872	0.0002	2.1023	0.0090	0.1749	0.0008	0.0551	0.0005	1365	4	1150	3	1039	4	1084	9	89%
LL169-42	0.80	0.0906	0.0002	2.1553	0.0129	0.1725	0.0010	0.0720	0.0015	1439	4	1167	4	1026	6	1405	29	87%
LL169-43	1.26	0.0978	0.0003	2.9935	0.0429	0.2210	0.0027	0.0870	0.0011	1583	6	1406	11	1287	14	1685	21	91%
LL169-46	1.83	0.0798	0.0002	1.4546	0.0056	0.1322	0.0004	0.0361	0.0003	1192	6	912	2	800	3	718	5	86%
LL169-48	1.12	0.0890	0.0003	2.6117	0.0251	0.2124	0.0016	0.0812	0.0007	1406	6	1304	7	1242	9	1578	14	95%
LL169-49	2.79	0.0958	0.0003	2.6642	0.0201	0.2014	0.0011	0.0466	0.0008	1544	6	1319	6	1183	6	920	15	89%
LL169-51	1.37	0.1326	0.0007	4.7085	0.0589	0.2560	0.0020	0.0936	0.0011	2133	9	1769	10	1470	10	1809	21	81%
LL169-52	0.69	0.1243	0.0021	3.9014	0.0665	0.2283	0.0013	0.1268	0.0024	2020	31	1614	14	1326	7	2414	43	80%
LL169-54	1.82	0.0948	0.0007	1.9397	0.0491	0.1461	0.0026	0.0362	0.0009	1524	14	1095	17	879	14	718	17	78%
LL169-55	0.36	0.0848	0.0002	2.0893	0.0168	0.1785	0.0012	0.0875	0.0008	1322	5	1145	6	1059	7	1695	15	92%
LL169-10	1.67	0.0772	0.0003	1.7193	0.0176	0.1612	0.0011	0.0271	0.0006	1128	13	1016	7	963	6	541	12	94%
LL169-61	1.02	0.0877	0.0005	2.2673	0.0388	0.1855	0.0022	0.0644	0.0010	1376	12	1202	12	1097	12	1262	18	90%
LL169-64	3.45	0.1009	0.0003	3.3528	0.0187	0.2408	0.0009	0.0693	0.0006	1643	10	1493	4	1391	5	1355	12	92%
LL169-65	2.96	0.1008	0.0002	3.5470	0.0159	0.2550	0.0011	0.0790	0.0012	1640	4	1538	4	1464	5	1537	23	95%

Table A3
(continued)

	Th/U	$^{207}Pb/^{206}Pb$ Ratio	1σ	$^{207}Pb/^{235}U$ Ratio	1σ	$^{206}Pb/^{238}U$ Ratio	1σ	$^{208}Pb/^{232}Th$ Ratio	1σ	$^{207}Pb/^{206}Pb$ Age (Ma)	1σ	$^{207}Pb/^{235}U$ Age (Ma)	1σ	$^{206}Pb/^{238}U$ Age (Ma)	1σ	$^{208}Pb/^{232}Th$ Age (Ma)	1σ	Con.
Unmodified, magmatic zircon																		
Porous domains																		
LL169-03	1.41	0.1154	0.0005	4.0648	0.0160	0.2558	0.0012	0.0888	0.0007	1887	7	1647	3	1468	6	1720	12	88%
LL169-67	1.22	0.0954	0.0006	2.6961	0.0204	0.2047	0.0008	0.0755	0.0008	1537	11	1327	6	1200	4	1472	15	89%
LL169-68	1.22	0.0872	0.0002	2.3319	0.0241	0.1936	0.0017	0.0811	0.0016	1365	5	1222	7	1141	9	1576	30	93%
LL169-69	0.70	0.0808	0.0002	1.9267	0.0110	0.1728	0.0009	0.0653	0.0008	1218	10	1090	4	1028	5	1278	15	94%
LL169-70	1.19	0.0957	0.0003	2.6890	0.0309	0.2029	0.0018	0.0627	0.0010	1543	7	1325	8	1191	10	1229	19	89%
LL169-71	2.50	0.0787	0.0002	1.2213	0.0092	0.1126	0.0009	0.0240	0.0003	1165	4	810	4	688	5	479	5	83%
LL169-79	1.21	0.0846	0.0003	1.9556	0.0146	0.1675	0.0009	0.0535	0.0004	1306	11	1100	5	998	5	1053	8	90%
LL169-81	1.42	0.1124	0.0003	4.0470	0.0322	0.2609	0.0019	0.0874	0.0010	1839	6	1644	6	1495	10	1693	18	90%
LL169-83	1.41	0.0806	0.0003	1.7308	0.0139	0.1555	0.0009	0.0376	0.0011	1213	6	1020	5	932	5	746	21	90%
LL169-85	1.51	0.0928	0.0003	2.3958	0.0179	0.1871	0.0011	0.0552	0.0006	1483	6	1241	5	1105	6	1086	11	88%
LL169-87	0.79	0.0852	0.0002	2.3154	0.0198	0.1969	0.0014	0.0735	0.0005	1320	6	1217	6	1159	7	1434	10	95%
LL169-90	1.14	0.0934	0.0005	2.5215	0.0215	0.1955	0.0010	0.0631	0.0008	1495	9	1278	6	1151	6	1237	15	89%
LL169-95	1.03	0.0956	0.0003	3.2149	0.0235	0.2437	0.0017	0.0863	0.0010	1540	5	1461	6	1406	9	1673	19	96%
LL169-96	1.84	0.0920	0.0003	2.4404	0.0231	0.1919	0.0014	0.0621	0.0008	1533	6	1255	7	1132	7	1217	15	89%
LL169-97	0.85	0.0952	0.0003	2.8291	0.0121	0.2155	0.0009	0.0757	0.0008	1532	6	1363	3	1258	5	1475	14	91%
LL169-98	0.37	0.0768	0.0002	1.2061	0.0069	0.1139	0.0005	0.0390	0.0007	1117	6	803	3	695	3	773	14	85%
LL169-86	1.11	0.0873	0.0021	2.0661	0.0632	0.1700	0.0010	0.0556	0.0015	1369	46	1138	21	1012	6	1094	28	88%
LL169-92	1.51	0.0779	0.0002	1.7240	0.0083	0.1605	0.0007	0.0423	0.0006	1144	5	1018	3	959	4	837	12	94%
Overgrowth/rims																		
LL169-19	1.22	0.0804	0.0003	1.1598	0.0141	0.1042	0.0009	0.0277	0.0004	1207	9	782	7	639	5	553	8	79%
LL169-28	1.73	0.0757	0.0002	1.1129	0.0043	0.1066	0.0003	0.0309	0.0002	1087	8	760	2	653	2	616	4	84%
LL169-53	0.67	0.0735	0.0002	1.5825	0.0073	0.1562	0.0006	0.0536	0.0004	1028	5	963	3	936	3	1056	7	97%
LL169-59	0.32	0.0725	0.0003	1.6475	0.0118	0.1648	0.0009	0.0637	0.0006	1000	9	989	5	983	5	1248	12	99%
LL169-62	0.23	0.0742	0.0002	1.2495	0.0075	0.1220	0.0006	0.0379	0.0004	1056	6	823	3	742	3	752	8	89%
LL169-75	0.72	0.0754	0.0002	1.4666	0.0088	0.1409	0.0006	0.0434	0.0004	1080	7	917	4	850	3	858	9	92%

TABLE A4

Hf isotopic compositions of different zircon in the altered gabbro

	$^{176}Hf/^{177}Hf$	1σ	$^{176}Lu/^{177}Hf$	1σ	$^{176}Yb/^{177}Hf$	1σ	Hf	Lu	Yb	Yb/Hf
Inclusion-free domains										
LL169-03	0.281928	0.000038	0.003284	0.000069	0.076773	0.001576	76296	2355	10221	0.13
LL169-06	0.281986	0.000035	0.004508	0.000046	0.079154	0.000349	76770	3142	10177	0.13
LL169-07	0.282002	0.000031	0.005776	0.000144	0.104216	0.002031	64214	3221	10885	0.17
LL169-14	0.281999	0.000033	0.003948	0.000114	0.078982	0.001394	74129	2822	10328	0.14
LL169-21	0.281838	0.000024	0.003516	0.000063	0.103188	0.001735	63288	1979	10967	0.17
LL169-23	0.281987	0.000025	0.004730	0.000032	0.114581	0.000841	56860	2483	11315	0.20
LL169-25	0.282000	0.000032	0.004000	0.000107	0.086530	0.002109	70969	2584	10517	0.15
Porous domains										
LL169-01	0.282076	0.000031	0.005183	0.000037	0.092594	0.000606	67471	3204	10696	0.16
LL169-04	0.282069	0.000028	0.003498	0.000020	0.080765	0.000836	74855	2393	10300	0.14
LL169-09	0.282079	0.000045	0.004161	0.000066	0.117784	0.001663	56159	2148	11354	0.20
LL169-10	0.282072	0.000031	0.005474	0.000048	0.162647	0.000666	43811	2132	12056	0.28
LL169-19	0.281915	0.000026	0.004822	0.000053	0.144241	0.001766	48170	2099	11814	0.25
LL169-22	0.281985	0.000031	0.006315	0.000043	0.196906	0.001712	37127	2125	12436	0.33
LL169-29	0.282069	0.000034	0.004617	0.000039	0.169625	0.002034	40473	1769	12251	0.30
LL169-30	0.282044	0.000030	0.004615	0.000033	0.148484	0.001596	45234	1974	11979	0.26
Overgrowth/rims										
LL169-08	0.282204	0.000035	0.005451	0.000034	0.190411	0.001323	38521	1898	12360	0.32
LL169-15	0.282185	0.000052	0.007988	0.000076	0.214715	0.001495	34522	2479	12574	0.36
LL169-24	0.282159	0.000039	0.006494	0.000018	0.236477	0.000981	31055	1866	12779	0.41

REFERENCES

Ayers, J. C., DeLaCruz, K., Miller, C., and Switzer, O., 2003, Experimental study of zircon coarsening in quartzite $\pm H_2O$ at 1.0 GPa and 1000 °C, with implications for geochronological studies of high-grade metamorphism: American Mineralogist, v. 88, n. 2–3, p. 365–376, https://doi.org/10.2138/am-2003-2-313

Campbell, L. S., Compston, W., Sircombe, K. N., and Wilkinson, C. C., 2014, Zircon from the East Orebody of the Bayan Obo Fe-Nb-REE deposit, China, and SHRIMP ages for carbonatite-related magmatism and REE mineralization events: Contributions to Mineralogy and Petrology, v. 168, n. 2, article 1041, https://doi.org/110.1007/s00410-014-1041-3

Chen, G. W., Yu, X. W., and Cheng, D. R., 1991, Research on the thermo-chemical condition of the Fe-Cu mineralization in the Lala deposit, Sichuan Province: Southwest Deposit Geology, v. 5, p. 43–51 (in Chinese).

Chen, W. T., and Zhou, M.-F., 2012, Paragenesis, stable isotopes, and molybdenite Re-Os isotope age of the Lala iron-copper deposit, Southwest China: Economic Geology, v. 107, n. 3, p. 459–480, https://doi.org/10.2113/econgeo.107.3.459

——— 2014, Ages and compositions of primary and secondary allanite from the Lala Fe-Cu deposit, SW China: implications for multiple episodes of hydrothermal events: Contributions to Mineralogy and Petrology, v. 168, n. 2, article 1043, p. 1031–1062, https://doi.org/10.1007/s00410-014-1043-1

——— 2015, Mineralogical and geochemical constraints on mobilization and mineralization of rare Earth elements in the Lala Fe-Cu-(Mo, REE) deposit, SW China: American Journal of Science, v. 315, n. 7, p. 671–711, https://doi.org/10.2475/07.2015.03

Chen, W. T., Zhou, M.-F., and Zhao, X.-F., 2013, Late Paleoproterozoic sedimentary and mafic rocks in the Hekou area, SW China: Implication for the reconstruction of the Yangtze Block in Columbia: Precambrian Research, v. 231, p. 61–77, https://doi.org/10.1016/j.precamres.2013.03.011

Chen, W. T., Sun W.-H., Wang, W., Zhao J.-H., and Zhou, M.-F., 2014, "Grenvillian" intra-plate mafic magmatism in the southwestern Yangtze Block, SW China: Precambrian Research, v. 242, p. 138–153, https://doi.org/10.1016/j.precamres.2013.12.019

Chen, Z. L., and Chen, S. Y., 1987, On the tectonic evolution of the west margin of the Yangzi Block: Chongqing, China, Chongqing Publishing House, 172 p. (in Chinese with English abstract).

Cherniak, D. J., and Watson, E. B., 2000, Pb diffusion in zircon: Chemical Geology, v. 172, n. 1–2, p. 5–24, https://doi.org/10.1016/S0009-2541(00)00233-3

Corfu, F., Hanchar, J. M., Hoskin, P. W. O., and Kinny, P. D., 2003, Atlas of zircon textures, *in* Hanchar, J. M., and Hoskin, P. W. O., editors, Zircon: Reviews in Mineralogy and Geochemistry, v. 53, n. 1, p. 469–500, https://doi.org/10.2113/0530469

Ewing, R. C., Meldrum, A., Wang, L., Weber, W. J., and Corrales, R. L., 2003, Radiation effects in zircon, *in* Hanchar, J. M., and Hoskin, P. W. O., editors, Zircon: Reviews in Mineralogy and Geochemistry, v. 53, n. 1, p. 387–420, https://doi.org/10.2113/0530387

Fu, B., Mernagh, T. P., Kita, N. T., Kemp, A. I. S., and Valley, J. W., 2009, Distinguishing magmatic zircon from hydrothermal zircon: A case study from the Gidginbung high-sulphidation Au-Ag-(Cu) deposit, SE Australia: Chemical Geology, v. 259, n. 3–4, p. 131–142, https://doi.org/10.1016/j.chemgeo.2008.10.035

Geisler, T., Pidgeon, R. T., Kurtz, R., Bronswijk, W. V., and Scheicher, H., 2003, Experimental hydrothermal alteration of partially metamict zircon: American Mineralogist, v. 88, n. 10, p. 1496–1513, https://doi.org/10.2138/am-2003-1013

Geisler, T., Burakov B. E., Zirlin, V., Nikolaeva, L., and Poml, P., 2005, A Raman spectroscopic study of high-uranium zircon from the Chernobyl "lava": European Journal of Mineralogy, v. 17, n. 6, p. 883–894, https://doi.org/10.1127/0935-1221/2005/0017-0883

Geisler, T., Schaltegger, U., and Tomaschek, F., 2007, Re-equilibration of zircon in aqueous fluids and melts: Elements, v. 3, n. 1, p. 43–50, https://doi.org/10.2113/gselements.3.1.43

Geng, Y .S., Yang, C. H., Du, L. L., Wang, X. S., Ren, L. D., and Zhou, X. W., 2007, Chronology and tectonic environment of the Tianbaoshan Formation: new evidence from zircon SHRIMP U-Pb age and geochemistry: Geological Review, v. 53, p. 556–563 (in Chinese with English abstract).

Gerdes, A., and Zeh, A., 2009, Zircon formation versus zircon alteration-new insights from combined U-Pb and Lu-Hf *in-situ* LA-ICP-MS analyses, and consequences for the interpretation of Archean zircon from the Central Zone of the Limpopo Belt: Chemical Geology, v. 261, n. 3–4, p. 230–243, https://doi.org/10.1016/j.chemgeo.2008.03.005

Guan, J. L., Zheng, L. L., Lui, J. H., Sun, Z. M., and Cheng, W. H., 2011, Zircons SHRIMP U–Pb dating of diabase from Hekou, Sichuan Province, China and its geological significance: Acta Geologica Sinica, v. 85, n. 4, p. 482–490 (in Chinese with English abstract).

Greentree, M. R., and Li, Z. X., 2008, The oldest known rocks in south-western China: SHRIMP U-Pb magmatic crystallization age and detrital provenance analysis of the Paleoproterozoic Dahongshan Group: Journal of Asian Earth Sciences, v. 33, n. 5–6, p. 289–302, https://doi.org/10.1016/j.jseaes.2008.01.001

Greentree, M. R., Li, Z. X., Li, X. H., and Wu, H. C., 2006, Late Mesoproterozoic to earliest Neoproterozoic basin record of the Sibao orogenesis in western South China and relationship to the assembly of Rodinia: Precambrian Research, v. 151, n. 1–2, p. 79–100, https://doi.org/10.1016/j.precamres.2006.08.002

Hay, D. C., and Dempster, T. J., 2009a, Zircon behavior during low-temperature metamorphism: Journal of Petrology, v. 50, n. 4, p. 571–589, https://doi.org/10.1093/petrology/egp011

——— 2009b, Zircon alteration, formation and preservation in sandstones: Sedimentology, v. 56, n. 7, p. 2175–2191, https://doi.org/10.1111/j.1365-3091.2009.01075.x

Hoskin, P. W. O., 2005, Trace-element composition of hydrothermal zircon and the alteration of Hadean zircon from the Jack Hills, Australia: Geochimica et Cosmochimica Acta, v. 69, n. 3, p. 637–648, https://doi.org/10.1016/j.gca.2004.07.006

Hoskin, P. W. O., and Schaltegger, U., 2003, The composition of zircon and igneous and metamorphic petrogenesis, *in* Hanchar, J. M., and Hoskin, P. W. O., editors, Zircon: Reviews in Mineralogy and Geochemistry, v. 53, p. 27–62, https://doi.org/10.2113/0530027

Hoskin, P. W. O., Kinny, P. D., Wyborn, D., and Chappell, B. W., 2000, Identifying accessory mineral saturation during differentiation in granitoid magmas: An integrated approach: Journal of Petrology, v. 41, n. 9, p. 1365–1396, https://doi.org/10.1093/petrology/41.9.1365

Hu, A., Zhu, B., Mao, C., Zhu, N., and Hunang, R., 1991, Geochronology of the Dahongshan Group: Chinese Journal of Geochemistry, v. 10, p. 195–203 (in Chinese with English abstract).

Jin, M. X., and Shen, S., 1998, Fluid features and metallogenic conditions in Lala copper deposit, Huili, Sichuan, China: Geological Science and Technology Information, v. 17, p. 45–48 (in Chinese with English abstract).

Kempe, U., Seltmann, R., Graupner, T., Rodionov, N., Sergeev, S. A., Matukov, D. I., and Kremenetsky, A. A., 2015, Concordant U-Pb SHRIMP ages of U-rich zircon in granitoids from the Muruntau gold district (Uzbekistan): Timing of intrusion, alteration ages or meaningless numbers: Ore Geology Reviews, v. 65, Part 1, p. 308–326, https://doi.org/10.1016/j.oregeorev.2014.10.007

Kerrich, R., and King, R., 1993, Hydrothermal zircon and baddeleyite in Val-Dor Archean mesothermal gold deposits: characteristics, compositions, and fluid-inclusion properties, with implications for timing of primary gold mineralization: Canadian Journal of Earth Sciences, v. 30, n. 12, p. 2334–2351, https://doi.org/10.1139/e93-203

Lee, J. K. W., Williams, I. S., and Ellis, D. J., 1997, Pb, U and Th diffusion in natural zircon: Nature, v. 390, p. 159–162, https://doi.org/10.1038/36554

Li, F. H., Tan, J. M., Shen, Y. L., Yu, F. X., Zhou, G. F., Pan, X. N., and Li, X. Z., 1988, The Presinian in the Kangdian area: Chongqing, China, Chongqing Publishing House, p. 396 (in Chinese with English abstract).

Lippmann, F., 1980, Phase diagrams depicting the aqueous solubility of binary mineral systems: Neues Jahrbuch fur Mineralogie, Abhandlungen, v. 139, n. 1, p. 1–25.

Liu, Y. S., Hu, Z. C., Gao, S., Günther, D., Xu, J., Gao, C. G., and Chen, H. H., 2008, *In situ* analysis of major and trace elements of anhydrous minerals by LA-ICP-MS without applying an internal standard: Chemical Geology, v. 257, n. 1–2, p. 34–43, https://doi.org/10.1016/j.chemgeo.2008.08.004

Ludwig, K. R., 2003, Isoplot 3.00: A Geochronological Toolkit for Microsoft Excel: Berkeley, California, Berkeley Geochronology Center.

Martin, L. A. J., Duchene, S., Deloule, E., and Vanderhaeghe, O., 2006, The isotopic composition of zircon and garnet: a record of the metamorphic history of Naxos, Greece: Lithos, v. 87, n. 3–4, p. 174–192. https://doi.org/10.1016/j.lithos.2005.06.016

Martin, L. A. J., Duchene, S., Deloule, E., and Vanderhaeghe, O., 2008, Mobility of trace elements and oxygen in zircon during metamorphism: Consequences for geochemical tracing: Earth and Planetary Science Letters, v. 267, n. 1–2, p. 161–174, https://doi.org/10.1016/j.epsl.2007.11.029

McGloin, M. V., Tomkins, A. G., Webb, G. P., Spiers, K., MacRae, C. M., Paterson, D., and Ryan, C. G., 2015, Release of uranium from highly radiogenic zircon through metamictization: The source of orogenic uranium ores: Geology, v. 44, n. 1, p. 15–18, https://doi.org/10.1130/G37238.1

Murakami, T., Chakoumakos, B. C., Ewing, R. C., Lumpkin, G. R., and Weber, W. J., 1991, Alpha-decay event damage in zircon: American Mineralogist, v. 76, n. 9–10, p. 1510–1532.

Pearce, N. J. G., Perkins, W. T., Westgate, J. A., Gorton, M. P., Jackson, S. E., Neal, C. R., and Chenery, S. P., 1997, A compilation of new and published major and trace element data for NIST SRM 610 and NIST SRM 612 Glass Reference Materials: Geostandards Newsletter, v. 21, n. 1, p. 115–144, https://doi.org/10.1111/j.1751-908X.1997.tb00538.x

Pelleter, E., Cheilletz, A., Gasquet, D., Mouttaqi, A., Annich, M., El Hakourd, A., Deloule, E., and Féraude, G., 2007, Hydrothermal zircons: a tool for ion microprobe U–Pb dating of gold mineralization (Tamlalt-Menhouhou gold deposit-Morocco): Chemical Geology, v. 245, n. 3–4, p. 135–161, https://doi.org/10.1016/j.chemgeo.2007.07.026

Putnis, A., 2002, Mineral replacement reactions: From macroscopic observations to microscopic mechanisms: Mineralogical Magazine, v. 66, n. 5, p. 689–708, https://doi.org/10.1180/0026461026650056

Rizvanova, N. G., Levchenkov, O. A., Belous, A. E., Bezmen, N. I., Maslenikov, A. N., Komarov, A. N., Makeev, A. F., and Levskiy, L. K., 2000, Zircon reaction and stability of the U-Pb isotope system during interaction with carbonate fluid: experimental hydrothermal study: Contributions to Mineralogy and Petrology, v. 139, n. 1, p. 101–114, https://doi.org/10.1007/s004100050576

Rubatto, D., Müntener, O., Barnhoorn, A., and Gregory, C., 2008, Dissolution-reprecipitation of zircon at low-temperature, high-pressure conditions (Lanzo massif, Italy): American Mineralogist, v. 93, n. 10, p. 1519–1529, https://doi.org/10.2138/am.2008.2874

Sinha, A. K., Wayne, D. M., and Hewitt, D. A., 1992, The hydrothermal stability of zircon: Preliminary experimental and isotopic studies: Geochimica et Cosmochimica Acta, v. 56, n. 9, p. 3551–3560, https://doi.org/10.1016/0016-7037(92)90398-3

Schneider, D. A., Senkowski, C., Vogel, H., Grasemann, B., Iglseder, Ch., and Schmitt, A. K., 2011, Eocene tectonometamorphism on Serifos (western Cyclades) deduced from zircon depth-profiling geochronology and mica thermochronology: Lithos, v. 125, n. 1–2, p. 151–172, https://doi.org/10.1016/j.lithos.2011.02.005

Schneider, D. A., Bachtel, J., and Schmitt, A. K., 2012, Zircon alteration in Wall Rock of Pamour and Hoyle Pond mines, Abitibi Greenstone Belt: Constraints on Timescales of fluid flow from dept-profiling techniques: Economic Geology, v. 107, n. 5, p. 1043–1072, https://doi.org/10.2113/econgeo.107.5.1043

Shentu, B. Y., 1997, Geological and geochemical characteristics of the Lala copper deposit and its formation model: Tethyan Geology, v. 21, p. 112–126. (in Chinese).

Sun, K., Shen, Y., Liu, G., Li, Z., and Pan, X., 1991, Proterozoic iron-copper deposits in central Yunnan Province: Wuhan, China, China University of Geoscience Press, 169 p. (in Chinese with English abstract).

Sun, S. S., and McDonough, W. F., 1989, Chemical and isotopic systematics of oceanic basalt: Implications for mantle composition and processes, *in* Saunders, A. D., and Norry, M. J., editors, Magmatism in the Ocean Basins: Geological Society, London, Special Publications, v. 42, p. 313–345, https://doi.org/10.1144/GSL.SP.1989.042.01.19

Sun, Y., and Liu, C., 1990, Mineralization mechanism of Lala copper deposit in Sichuan Province: Journal of Chengdu College of Geology, v. 17, p. 1–9 (in Chinese with English abstract).

Sun, W. H., Zhou, M. F., Gao, J. F., Yang, Y. H., Zhao, X. F., and Zhao, J. H., 2009, Detrital zircon U-Pb geochronological and Lu-Hf isotopic constraints on the Precambrian magmatic and crustal evolution of the western Yangtze Block, SW China: Precambrian Research, v. 172, n. 1–2, p. 99–126, https://doi.org/10.1016/j.precamres.2009.03.010

Taylor, R. J. M., Clark, C., Fitzsimons, I. C. W., Santosh, M., Hand, M., Evans, N., and McDonald, B., 2014, Post-peak, fluid-mediated modification of granulite facies zircon and monazite in the Trivandrum Block, southern India: Contributions to Mineralogy and Petrology, v. 168, p. 1044–1060, https://doi.org/10.1007/s00410-014-1044-0

Tomaschek, F., Kennedy, A. K., Villa, I. M., Lagos, M., and Ballhaus, C., 2003, Zircons from Syros, Cyclades, Greece-recrystallization and mobilization of zircon during high-pressure metamorphism: Journal of Petrology, v. 44, n. 11, p. 1977–2002, https://doi.org/10.1093/petrology/egg067

Tu, X. L., Zhang, H., Deng, W. F., Ling, M. X., Liang, H. Y., Liu, Y., and Sun, W. D., 2011, Application of RESOlution *in-situ* laser ablation ICP-MS in trace element analyses: Geochimica, v. 10, p. 83–98 (in Chinese with English Abstract).

Van Lankvelt, A., Schneider, D. A., Biczok, J., McFarlane, C. R. M., and Hattori, K., 2016, Decoding zircon geochronology of igneous and alteration events based on chemical and microstructural features: A study from the western Superior Province, Canada: Journal of Petrology, v. 57, n. 7, p. 1309–1334, https://doi.org/10.1093/petrology/egw041

Wang, X.-L., Coble, M. A., Valley, J. W., Shu, X. J., Kitajima, K., Spicuzza, M. J., and Sun, T., 2014, Influence of radiation damage on late Jurassic zircon from southern China: Evidence from *in situ* measurements of oxygen isotopes, laser Raman, U-Pb ages, and trace elements: Chemical Geology, v. 389, 122–136, https://doi.org/10.1016/j.chemgeo.2014.09.013

Yu, Z., and Liu, C., 1988, One allosource-comineralization ore deposit-A discussion on the genesis of Lala ore deposit in Sichuan, SW China: Acta Petrologica Sinica, v. 2, p. 78–87 (in Chinese with English abstract).

Yuan, H. L., Gao, S., Dai, M.-N., Zong, C. L., Günther, D., Fontaine, G. H., Liu, X.-M., and Diwu, C.R., 2008, Simultaneous determinations of U-Pb age, Hf isotopes and trace element compositions of zircon by excimer laser-ablation quadrupole and multiple-collector ICP-MS: Chemical Geology, v. 247, n. 1–2, p. 100–118, https://doi.org/10.1016/j.chemgeo.2007.10.003

Zhao, X. F., and Zhou, M. F., 2011, Fe-Cu deposits in the Kangdian region, SW China: A Proterozoic IOCG (iron-oxide-copper-gold) metallogenic province: Mineralium Deposita, v. 46, n. 7, p. 731–7477, https://doi.org/10.1007/s00126-011-0342-y

Zhao, X. F., Zhou, M. F., Li, J. W., Sun, M., Gao, J. F., Sun, W. H., and Yang, J. H., 2010, Late Paleoproterozoic to early Mesoproterozoic Dongchuan Group in Yunnan, SW China: Implications for tectonic evolution of the Yangtze Block: Precambrian Research, v. 182, n. 1–2, p. 57–69, https://doi.org/10.1016/j.precamres.2010.06.021

Zhou, M. F., Yan, D. P., Kennedy, A. K., Li, Y., and Ding, J., 2002, SHRIMP U-Pb zircon geochronological and geochemical evidence for Neoproterozoic arc-magmatism along the western margin of the Yangtze Block, South China: Earth Planet and Science Letter, v. 196, n. 1–2, p. 51–67, https://doi.org/10.1016/S0012-821X(01)00595-7

Zhou, M. F., Ma, Y., Yan, D. P., Xia, X., Zhao, J. H., and Sun, M., 2006, The Yanbian Terrane (Southern Sichuan Province, SW China): A Neoproterozoic arc assemblage in the western margin of the Yangtze Block: Precambrian Research, v. 144, n. 1–2, p. 19–38, https://doi.org/10.1016/j.precamres.2005.11.002

Zhou, M. F., Zhao, X. F., Chen, W. T., Li, X. C., Wang, W., Yan, D. P., and Qiu, H. N., 2014, Proterozoic Fe-Cu metallogeny and supercontinental cycles of the southwestern Yangtze Block, southern China and northern Vietnam: Earth-Science Reviews, v. 139, p. 59–82, https://doi.org/10.1016/j.earscirev.2014.08.013